molecular pharmaceutics

pubs.acs.org/molecularpharmaceutics

Article

Embedding Dynamics in Intrinsic Physicochemical Profiles of Market-Stage Antibody-Based Biotherapeutics

Giuseppe Licari, Kyle P. Martin, Maureen Crames, Joseph Mozdzierz, Michael S. Marlow, Anne R. Karow-Zwick, Sandeep Kumar,* and Joschka Bauer*

Cite This: *Mol. Pharmaceutics* 2023, 20, 1096−1111

Read Online

ACCESS | Metrics & More | Article Recommendations | Supporting Information

ABSTRACT: Adequate stability, manufacturability, and safety are crucial to bringing an antibody-based biotherapeutic to the market. Following the concept of holistic in silico developability, we introduce a physicochemical description of 91 market-stage antibody-based biotherapeutics based on orthogonal molecular properties of variable regions (Fvs) embedded in different simulation environments, mimicking conditions experienced by antibodies during manufacturing, formulation, and in vivo. In this work, the evaluation of molecular properties includes conformational flexibility of the Fvs using molecular dynamics (MD) simulations. The comparison between static homology models and simulations shows that MD significantly affects certain molecular descriptors like surface molecular patches. Moreover, the structural stability of a subset of Fv regions is linked to changes in their specific molecular interactions with ions in different experimental conditions. This is supported by the observation of differences in protein melting temperatures upon addition of NaCl. A DEvelopability Navigator In Silico (DENIS) is proposed to compare mAb candidates for their similarity with market-stage biotherapeutics in terms of physicochemical properties and conformational stability. Expanding on our previous developability guidelines (Ahmed et al. *Proc. Natl. Acad. Sci.* **2021**, *118* (37), e2020577118), the hydrodynamic radius and the protein strand ratio are introduced as two additional descriptors that enable a more comprehensive in silico characterization of biotherapeutic drug candidates. Test cases show how this approach can facilitate identification and optimization of intrinsically developable lead candidates. DENIS represents an advanced computational tool to progress biotherapeutic drug candidates from discovery into early development by predicting drug properties in different aqueous environments.

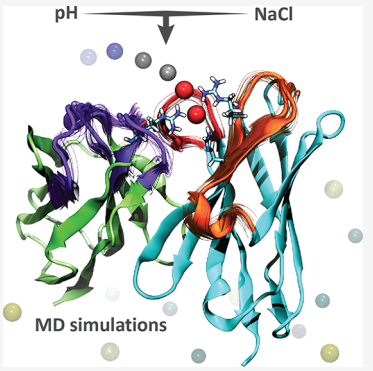

KEYWORDS: *biotherapeutics, protein flexibility, molecular dynamic simulations, ionic effects, physicochemical profile*

INTRODUCTION

Antibody-based biotherapeutics have emerged as one of the fastest-growing class of pharmaceuticals, covering multiple therapeutic areas.[1−3] Despite rapid industrialization, there are still several hurdles to successfully discover, develop, and manufacture biotherapeutic products at a commercial scale. Although there has been a trend of lowering attrition rates in preclinical and clinical stages,[4] only one in five biotherapeutic drug candidates that enter clinical trials survives through phases I, II, and III and eventually wins approval from regulatory agencies.[5] In addition to an optimal binding affinity toward the antigen, an antibody-based drug candidate must satisfy several other requirements in terms of safety, efficacy, and chemistry, manufacturing, and controls (CMC).[6−9] These challenges are further enhanced by the arrival of multi-specific antibody-based biotherapeutic candidates, which are still poorly understood due to their more complex structural formats.[10] Increasing drug development costs have promoted development of new in silico methods to support the selection and optimization of biologic drug candidates not only for function but also for "developability", i.e., the intrinsic ability of a drug candidate to be stable, manufacturable, safe, and pharmacologically effective.[9,11,12] Early selection of a good-to-develop drug candidate suitable for company-specific drug development platforms can help reduce the cost, time, and risk of failure at the later stages.

Increase in the availability of monoclonal antibody (mAb) experimental characterizations, access to accurate structural information, and homology modeling (HM) capabilities have fostered the development of computational approaches to address several developability aspects of biotherapeutics.[6] In silico evaluations do not require any material and can be performed either in parallel to or ahead of the experimental evaluations to support drug discovery, as shown by several works describing the prediction of experimental properties.[13−25] However, these tools often tackle individual aspects of

Received: October 3, 2022
Revised: December 10, 2022
Accepted: December 12, 2022
Published: December 27, 2022

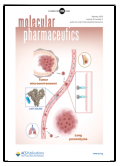

https://doi.org/10.1021/acs.molpharmaceut.2c00838
Mol. Pharmaceutics 2023, 20, 1096−1111

developability and do not take into consideration that the optimization of one antibody feature may potentially have detrimental effects on other properties.

Holistic in silico developability guidelines, which consider multiple aspects of antibody developability, are still scarce and not widely established. One example called Developability Index[26] provides a way to rank mAb candidates using a combination of only two characteristics: the spatial aggregation propensity (SAP) score of the complementary-determining regions (CDRs)[27] and the protein net charge of the full-length mAb. Another strategy highlights candidates similar to clinical-stage antibodies in terms of their computed biophysical properties (Therapeutic Antibody Profiler, TAP).[28] This tool tests homology models of the variable regions of antibody drug candidates against those of a set of clinical-stage antibody therapeutics using five metrics extracted from the reference structures. Similar molecular descriptors as in TAP were used in another work aimed at establishing profiling rules of clinical-stage antibody therapeutics.[29] In this case, the molecular descriptors were selected and evaluated to be predictive for aggregation, pharmacokinetics, and solution behavior. Previously, we have built an intrinsic physicochemical profile of 77 market-stage antibody-based therapeutics using variable region (Fv) homology models.[30] The term "market stage" should not be confused with "marketing or sales" aspects of biotherapeutics. Availability of an antibody-based biotherapeutic in the market is the final milestone in a journey that started with its discovery as a potential drug candidate and passed through all the stages of product and process development, clinical trials, regulatory approval, and commercial-scale manufacturing. While regulatory decisions for approval of biotherapeutics are often made on a case-to-case basis after a thorough analysis of risks versus benefits, there are some common characteristics among the marketed drug products. For example, all of them have been shown to be safe, effective, possess low (or no) target mediated or non-mechanism toxicity, and have acceptable pharmacology. Moreover, manufacturers of these biotherapeutics may have encountered several hurdles during their drug product development, process validation, and scale-up, but these hurdles did not prove insurmountable (see discussion in ref 30). Our previous work was focused on static homology-based models, excluding effects due to their conformational flexibility. Moreover, the workflow included only a single condition with fixed pH and ionic strength, whereas biotherapeutic drug candidates need to withstand various conditions during production, purification, storage, and in vivo upon administration.[6]

The physicochemical properties and solution behaviors of biotherapeutic drug candidates are highly dependent on their intrinsic conformational dynamics and on the environment conditions.[31] The use of a single static-energy-minimized antibody conformation is therefore a simplification of a complex conformational landscape that responds to the changes in the environmental conditions of the antibody molecule as it passes through various stages of formulation, manufacturing, and in vivo administration. Moreover, homology models generated using crystal structure templates may keep imprints from the template, suffer from crystal packing effects, and not accurately represent the dominant conformation of the antibody in solution.[31,32] For these reasons, it is desirable that in silico methods include, wherever feasible, conformational ensembles accessible to the antibody candidates.[15,33−35]

In this work, we have obtained new intrinsic physicochemical profiles of current market-stage antibodies by simulating conformational flexibilities of their Fv regions via all-atom explicit solvent molecular dynamics (MD). The simulations were performed at four conditions relevant to their solution behaviors at physiological, manufacturing, formulation, and downstream processing, therefore providing a broader in silico characterization of the market-stage antibody-based biotherapeutics at specific pH values and ionic strengths encountered during diverse research and development phases and in vivo. This profile, called here DEvelopability Navigator In Silico (DENIS), embedded MD and showed improved discriminatory characteristics when compared to using static homology models. The analysis of the simulation trajectories in different conditions provided insights into the stability of the variable regions of market-stage biotherapeutics in the presence/absence of ions and at different pH values.

MATERIALS AND METHODS

Sequence Collection of Market-Stage Antibody-Based Biotherapeutics. The set of market-stage biotherapeutics used in this work includes 12 new biotherapeutics (crizanlizumab, emapalumab, enfortumab vedotin, eptinezumab, inebilizumab, isatuximab, polatuzumab vedotin, ravulizumab, risankizumab, romosozumab, sacituzumab govitecan, and teprotumumab) that were approved by June 2020, in addition to the 79 Fvs from 77 market-stage biotherapeutics used in our previous work.[30] All available sequences were extracted from WHO,[36] TABS,[37] or IMGT.[38] Table S1 shows the publicly available information on all the 89 biotherapeutics studied in this report. The information compiled here includes the generic names, molecular formats, heavy and light chain isotypes, and formulations. Note that some of the information in this table was also previously disclosed in the Supplementary Material for our previous publication.[30]

Of the 89 market-stage biotherapeutics, 87 are monospecific antibodies and 2 are bispecific antibodies (emicizumab and blinatumomab, accounting for the two additional Fv regions in the dataset). The use of market-stage antibody-based biotherapeutics as references for holistic in silico developability guidelines is justified by the fact that drug products in the market have already been developed to withstand different physicochemical stresses experienced by the drug substance during manufacturing, shipping, storage, and administration. Therefore, information on whether a drug candidate has similar or better intrinsic physicochemical characteristics as the market-stage ones can be particularly useful toward its progression during discovery and the development cycle. However, due to the complex nature of biotherapeutics behavior, an in silico similarity to this reference set does not guarantee a successful journey of a candidate to the market. Instead, this profile should be used as an advisory for potentially optimizing the drug candidates whose intrinsic physicochemical parameters show significant deviations.

Preparation of Homology-Based Molecular Models. Molecular models of 91 Fv regions from 89 market-stage mAbs were obtained via homology modeling using the Antibody Modeler module implemented in Molecular Operating Environment (MOE) 2020[39] with a default Amber10: EHT force field. Solvation was included using the Generalized Born implicit model[40] with internal and external dielectric values set respectively to 4 and 80 and the non-bonded interaction tapered to zero between 10 and 12 Å. C-termini of the Fv light and heavy chains were amidated to have a neutral charge. The CCG (Chemical Computing Group) antibody annotation scheme was used throughout the work. The generated models underwent the

https://doi.org/10.1021/acs.molpharmaceut.2c00838
Mol. Pharmaceutics 2023, 20, 1096−1111

default structure preparation protocol in MOE to remove any errors and adjust their protonation states to the final desired pH and ion concentration. All structures were energy minimized below a 10^{-6} kcal/mol/Å^2 root mean square gradient threshold. All Fv regions were prepared in four different conditions, which were devised to mimic their solution behaviors at physiological, formulation processing, and low pH hold conditions during the viral inactivation step of biomanufacturing. The conditions differ in pH values and ion (NaCl) concentration (Table 1). The

Table 1. Conditions Used for Homology Modeling and MD Simulations to Mimic the Solution Behaviors of Market-Stage Biotherapeutics Variable Regions at Physiological, Formulation Processing, and Low pH Hold (Viral Inactivation Step) Conditions during Manufacturing[a]

condition tag	pH	[NaCl] (mM)
C1 (physiological)	7.4	137
C2 (formulation, no NaCl)	6.0	0
C3 (formulation, with NaCl)	6.0	150
C4 (viral inactivation step)	3.5	0

[a]The protonation state of each mAb was estimated at the beginning of the simulation and was kept fixed thereafter.

protonation state was determined using the Protonate 3D function[41] in MOE. After the homology modeling workflow, six antibodies (bezlotoxumab, cemiplimab, durvalumab, fremanezumab, racotumomab, rituximab) presented at least one *cis*-peptide bond, originating from the crystal structures used as modeling templates.[42] After repeating the protocol for obtaining conformation-averaged molecular descriptors (see next paragraphs) on bezlotoxumab with fixed *cis*-peptide bonds, no significant differences were observed, highlighting that within the simulation time, the presence of a few *cis*-peptide bonds does not significantly influence the relevant properties used in this work (Figure S1).

MD Simulations. All classical MD simulations were performed using NAMD2 and NAMD3, for equilibration and production runs, respectively.[43] The fully atomistic CHARMM36m force field[44] was used for protein, and the standard TIP3P model[45] was used for water. Nonbonded interactions were calculated with a cutoff of 12 Å, with a switching function starting at 10 Å. Particle mesh Ewald (PME)[46] was used to account for long-range electrostatic interactions with a grid density of 1 Å^{-3} and a PME interpolation order of 6. Rigid bonds for all hydrogen atoms were enforced using the SHAKE algorithm.[47] All simulations used for analysis were performed using periodic boundary conditions in the NPT ensemble (constant number of particles, pressure, and temperature), which was maintained by a Nosé−Hoover−Langevin piston and a Langevin thermostat (1 atm, period: 50 fs, decay: 25 fs, damping coefficient: 1.0 ps^{-1}).[48,49] The sizes of the rectangular box varied according to protein size, ensuring a minimum distance of 17 Å from the protein to each face of the box. The simulation timestep was set to 2 fs. Lennard-Jones forces were updated at every timestep, whereas PME forces were updated every two timesteps. All Fvs were equilibrated following an extensive multistep protocol: (i) 2000 steps of minimization followed by 20 ps simulation with a fixed periodic cell (NVT) and restraining all but water molecules with a high force constant (10 kcal/mol·Å^2); (ii) 20 ps in NPT restraining all but water molecules with the same force constant as in (i); (iii) additional 20 ps restraining only the protein and keeping the force constant as in (i); (iv) 100 ps restraining only the protein heavy atoms with a lower force constant (2.5 kcal/mol·Å^2); (v) 100 ps restraining only the protein backbone with the same force constant as in (iv); (vi) 100 ps restraining the protein backbone with a force constant of 1.0 kcal/mol·Å^2; and (vii) 100 ps without any restrains. This protocol ensures the thermal equilibration of the protein while avoiding large structural rearrangements that improperly alter the initial homology model. The total volume of the simulation cell after the equilibration ranged between 460 and 560 nm^3, with a total number of atoms varying between ∼45,900 and ∼51,100. The coordinates and velocities in the last snapshot of step (7) were used to start the simulation in production mode, which then were used for analysis. These final unrestrained trajectories ran for 200 ns for each mAb. The total simulation time sums up to ∼73 μs considering all 91 mAbs in all four conditions. The equilibration of the simulation systems was examined by monitoring the total energy, temperature, and pressure. Moreover, the root mean square deviation (RMSD) of the variable regions calculated in the 20−110 ns and in the 110−200 ns time ranges was extracted for each system at each condition and showed that there is no significant rearrangement of the protein conformations after the first 20 ns of equilibration (Figure S2).

Analysis of the trajectories was performed in VMD[50] using custom scripts. The final trajectories were prepared by centering the protein in the center of the box and aligning all frames to the position of the alpha carbon atoms in the first frame. The RMSD and root mean square fluctuation (RMSF) were calculated in VMD using the *measure rmsd/rmsf* functions by selecting only the alpha carbon atoms of all amino acids (Table S2). Unique H-bonds along the entire production trajectories were identified using a donor−acceptor distance cutoff of 3 Å and an angle cutoff of 20°; the cutoffs were increased to 4 Å and 60° when the acceptor was chlorine anion. Radial distribution functions were calculated using the *measure gofr* function implemented in VMD.[51] The variable region in nimotuzumab shows a peculiar behavior during the simulations with greater fluctuations in comparison to the variable regions from other biotherapeutics (Figure S3). The reason is ascribed to a disordered N-terminal in the heavy chains (Q1 to G8), with a local RMSF greater than ∼10 Å in all the four simulation conditions. The crystal structure of nimotuzumab (Protein Data Bank (PDB)[52] entry 3GKW)[53] also shows that its N-terminal is disordered, as the five N-terminal residues (Q1 to Q5) were not resolved due to smears in the electron density map. Other studies involving MD simulations of nimotuzumab did not report this effect, probably because of shorter simulation times, which did not allow for a more extensive observation of the disordered N-terminal.[53−55]

Calculation of Molecular Descriptors. For each Fv, protein properties were calculated using the energy-minimized homology models and the trajectories from the simulations. For the latter, the last 180 ns of the trajectories was used, since a preliminary analysis for three antibodies (burosumab, crizanlizumab, and denosumab) showed that there is still a significant change for protein properties in the first few nanoseconds (Figure S4A). Moreover, this analysis showed that it is not necessary to use all snapshots saved during the MD simulation to obtain converged averages for protein properties. For this work, it was sufficient to consider 300 snapshots along the 200 ns simulation (∼0.6 ns timestep, Figure S4B). Before calculating molecular descriptors, all protein snapshots went through the MOE structure preparation protocol to set the partial charges to

https://doi.org/10.1021/acs.molpharmaceut.2c00838
Mol. Pharmaceutics 2023, 20, 1096−1111

the default Amber10: EHT force field. Since the simulations were performed using the CHARMM36m force field, this procedure allows for the electrostatic terms in the molecular descriptors to be compatible with our previous work.[30] The protonation state was also re-evaluated for each protein snapshot at the target pH and NaCl concentration in the conditions C1−C4. A short minimization to a shallow 1.0 kcal/mol/Å^2 gradient threshold assured that there were no clashes and strains in the protein system.

To compare molecular descriptors obtained through HM and MD simulations in different simulation conditions, changes for relevant descriptors (d) were calculated as the mean percentage error (MPE) and mean absolute percentage error (MAPE) according to

$$\frac{100\cdot\sum_{i=1}^{n}\Delta^i/d^i_{\mathrm{MD}}}{n} \tag{1}$$

where $\Delta^i = (d^i_{\mathrm{MD}} - d^i_{\mathrm{HM}})$ or $\Delta^i = |d^i_{\mathrm{MD}} - d^i_{\mathrm{HM}}|$ for MPE and MAPE, respectively, with i running over all Fv regions ($n = 91$). Similarly, descriptors obtained from MD simulations at different simulation conditions were compared using

$$\frac{100\cdot\sum_{i=1}^{n}\Delta^i/d^i_{\mathrm{MD\_Cref}}}{n} \tag{2}$$

with $\Delta^i = (d^i_{\mathrm{MD\_Cref}} - d^i_{\mathrm{MD\_Cx}})$ or $\Delta^i = |d^i_{\mathrm{MD\_Cref}} - d^i_{\mathrm{MD\_Cx}}|$ for MPE and MAPE, respectively, and subscript Cref indicating the condition chosen as reference for the comparison. MAPE estimates the antibody-wise absolute change in properties. MPE gives additional information of the sign of the overall change, showing the possible existence of a general behavior for the whole set of Fv regions. To isolate the effect of ions, MAPE and MPE were calculated between conditions C2 and C3 (without/with NaCl and pH fixed at 6.0). Likewise, the effect of pH was considered by obtaining MAPE/MPE between conditions C2 and C4 (pH 6.0 and 3.5, no NaCl).

Unique Molecular Descriptors and Scoring Metrics. All 125 protein properties available in MOE 2020 were extracted during the analysis step to be considered for the final physicochemical profiles. The features reporting outlier values in the homology models, e.g., backbone bond torsion outlier, or possible *cis*-peptide bonds were excluded (in total six descriptors), as they carry no useful information to characterize the Fv regions. The descriptors containing the length on the CDRs were also disregarded (in total seven descriptors). Two descriptor combinations were instead added as previously introduced.[30] The first is equal to the ratio of surface areas of positively and negatively charged patches to that of hydrophobic patches ("RP"), whereas the second is equal to the ratio of dipole moment to hydrophobic moment ("RM"). The torsion angle between HC and LC ("HL angle)" and the distance between HC and LC ("dc distance)" from ABangle[56] implemented in MOE were used to describe the relative orientation between antibody variable domains but were not used for the construction of the physicochemical profiles because these descriptors carry a geometrical rather than physicochemical meaning.

Out of the final 114 descriptors, 97 showed a variance higher than 1% among Fv regions and along the trajectories in all simulated conditions. Moreover, an initial analysis was used to remove highly correlated descriptors with Pearson correlation coefficients higher than 0.75, reducing the number of molecular features down to 23−25 per simulated condition. To further half the number of descriptors, an agglomerative hierarchical clustering in SciPy[57] was applied to cluster the descriptors in 12 groups according to their pairwise correlation coefficients (Figures S5−S8).[30] The "average" method in the linkage function was used to calculate the distance between the newly formed clusters. One descriptor was selected as representative of each cluster resulting in a total of 13 descriptors. In an effort to further reduce the molecular descriptors and obtain only the most uncorrelated intrinsic properties, a statistically significant correlation between these 13 descriptors was considered using the rule of thumb $|r_{ij}| \geq \frac{2}{\sqrt{n}}$, where r_{ij} is the correlation coefficient between descriptors i and j and n is the total number of samples ($|r_{ij}| = 0.21$ for 91 Fvs in this work).[58] For each descriptor, the number of times that the descriptor was uncorrelated with another was counted in all simulated conditions and used as a ranking score (Figure S9). This exercise allowed for a sub-selection of descriptors that showed smaller inter-descriptor correlation. The eight computed descriptors that showed the highest frequency (f) of uncorrelation were hydrophobic imbalance ($f = 42$), protein helix ratio ($f = 42$), protein strand ratio ($f = 42$), ratio of dipole to hydrophobic moment ($f = 41$), buried surface area between LC and HC ($f = 41$), structure-based pI ($f = 40$), hydrodynamic ratio ($f = 35$), and ratio of charged to hydrophobic patches ($f = 33$). The protein helix ratio was also removed from the final descriptor because the helix content in Fv regions is low (below ∼5% of amino acids) and secondary structure information is already captured in the protein strand ratio.

Z-scores for each descriptor were computed as

$$Z_i = (x_{ij} - \mu_i)/\sigma_i \tag{3}$$

with index i and j running along all considered descriptors and mAbs, respectively, and μ and σ being the mean and standard deviation of the ith descriptor. The variants are ranked using the Z-distance metric calculated using the associated Z-scores as

$$\sqrt{\sum_i Z_i^2} \tag{4}$$

where the summation runs over the unique sub-selected descriptors.[30]

EXPERIMENTAL DATA

Thermal stability analysis of a subset of 38 market-stage antibodies was performed with a QuantStudio 5 RT-PCR system (Applied Biosystems, Waltham, Massachusetts). Protein samples in 10 mM histidine pH 6 with either 2 or 150 mM NaCl were diluted to a final concentration of 0.4 mg/mL and mixed with 6× SYPRO Orange (Invitrogen) and sealed in a 96-well PCR plate. The temperature was increased from 25 to 95 °C at a ramp rate of 1 °C/min. Samples were excited at 470 ± 15 nm and emission signals collected at 586 ± 11 nm. Fluorescence signals were plotted against temperature to generate melting curves. The local maxima of the first derivative of melting curves were taken as the T_m by using an in-house Python script.

RESULTS

pH Has a Greater Impact on Fv Conformational Stability than the Presence of NaCl. As a first glance into the effect of dynamics on the Fv regions of the market-stage biotherapeutics, the RMSD for all the 91 Fvs was extracted in the four different solution conditions (Table 1). The general trend

https://doi.org/10.1021/acs.molpharmaceut.2c00838
Mol. Pharmaceutics 2023, 20, 1096−1111

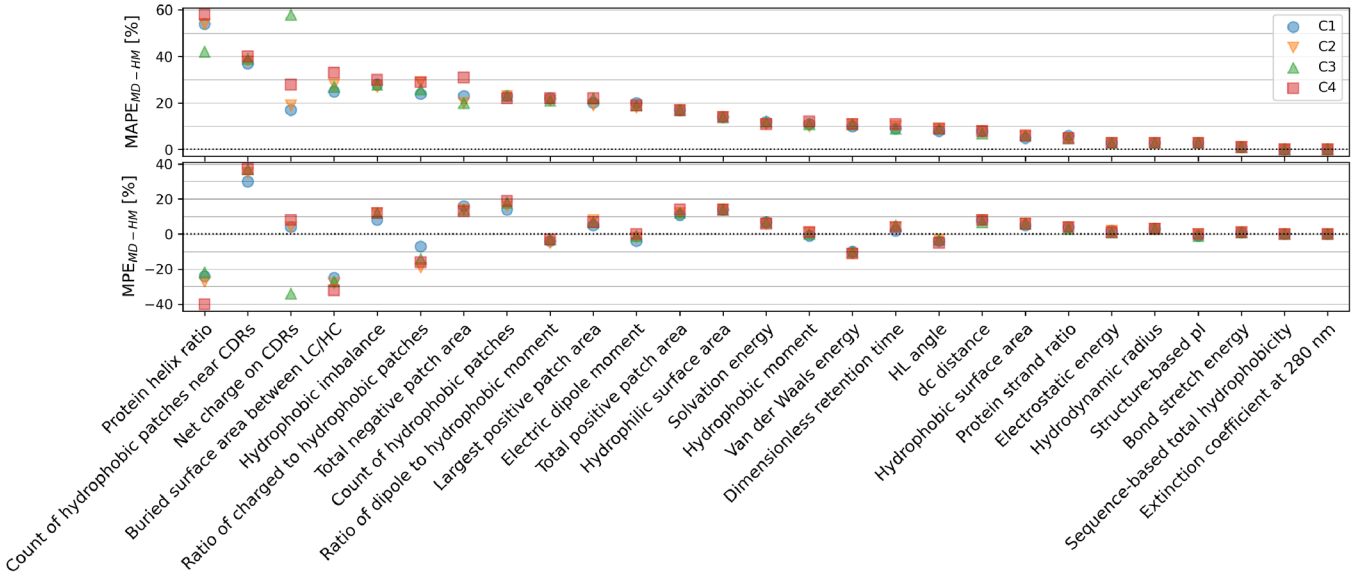

Figure 1. Effect of MD simulations on the molecular descriptors obtained as percentage change between values extracted from the MD simulations and from the energy-minimized homology models (HM) for all simulated conditions (C1: blue, C2: orange, C3: green, C4: red). The mean percentage error (MPE) and mean absolute percentage error (MAPE) were obtained through eq. 1 as averages along all Fv regions (Table S4). MAPE estimates the antibody-wise absolute change in properties. MPE gives additional information of the sign of the overall change, highlighting the possible existence of a general behavior for the whole set of Fv regions. The molecular descriptors were arranged in descending order according to MAPE.

shows that Fv regions fluctuate significantly in the first ∼20 ns, allowing for the initial homology models to relax toward a more conformationally stable configuration (Figure S15 and Table S2). The data indicate that the physiological conditions (C1: pH 7.4 and 137 mM NaCl) give rise to smaller conformational fluctuations in the Fv regions. On the other end, the low pH condition used at the viral inactivation step during manufacturing (C4: pH 3.5 and no added NaCl; low pH hold) shows greater conformational fluctuations indicating pH-induced destabilization. This observation is in line with the usually increased antibody aggregation due to protein denaturation at low pH hold during virus inactivation.[59] The two formulation conditions, C2 and C3 (pH 6 without or with added NaCl), show intermediate conformational flexibility. The pH therefore has a greater impact on the general structure stability of the Fv regions than the presence or absence of ions. Specific regions of higher fluctuation shown in RMSF profiles (Figure S15) coincide with the more flexible loops, particularly with CDR-H3 or with N- and C-termini, as described in the literature.[60,61]

Values of Physicochemical Descriptors Can Differ Significantly between Conformational Ensembles and Energy-Minimized Homology Models. The distributions of molecular descriptors and the MAPE for the Fv regions showing a correlation lower than 0.75 are reported in Figure 1 (see distribution plots in Figure S16 and a complete list of absolute and difference values in Tables S3 and S4). A few descriptors such as the structure-based pI or the hydrodynamic radius do not show changes after the simulations (MAPE <5%). The protein helix ratio, defined as the number of amino acids in helical conformation divided by the total number of amino acids and expressed in percentage, changes by up to ∼60% in C4. However, since the protein helix ratio is in general below ∼5% for all Fv regions, the relative change between static and MD simulation becomes prone to noise and gives rise to large differences. On the other hand, many other descriptors change significantly when the protein dynamics is taken into consideration. The salient ones are described below.

The surface patches obtained through the conformational ensembles are generally and systematically larger than in homology models (17−31% MAPE, +5−19% MPE), indicating that the relaxation allows for the formation of larger and more stable patches. In particular, the number of hydrophobic patches near CDRs increases by up to ∼40%. The standard deviations for patches are systematically higher for static models by 5 to 25% (Table S3). Therefore, distributions are narrower after the simulations, allowing for more converged molecular patches. Notably, the increase in hydrophobic patches is larger than the increase in charged patches, causing an overall decrease in the ratio of surface areas of the charged to hydrophobic patches (RP) by −7 to −19% (MPE). These changes reveal that MD simulations provide greater insights into properties of the molecular surfaces than the use of energy-minimized homology-based models alone. It was already discussed in previous works that hydrophobicity strongly depends on the conformation of the antibody, with conformational sampling improving the correlation with experimental values.[62]

The hydrophobic imbalance (HI) also shows a significant increase in all simulated conditions (MAPE ∼28%). This descriptor was devised to characterize the anisotropy in the hydrophobic residue distributions on the surface of a protein.[63] An increase in this value translates into more asymmetric distributions of hydrophobic residues on the molecular surface. Other molecular descriptors such as the electric dipole moment or the hydrophobic moment show significant variations in absolute terms (MAPE between 10 and 20%) but almost zero MPE, showing an antibody-dependent rather than a systematic change across all antibodies.

After the MD simulations, the buried surface area between LC and HC ($BSA_{VL:VH}$) shows a systematic reduction of 25 and 32% in C1 and C4, respectively (MAPE is equal to |MPE|). One reason for such change is ascribed to the lack of structural support from the constant region during the Fv simulations, as C_{H1} and C_L can stabilize interdomain orientation, significantly altering the binding interface of the antibody.[64,65] However,

https://doi.org/10.1021/acs.molpharmaceut.2c00838
Mol. Pharmaceutics 2023, 20, 1096−1111

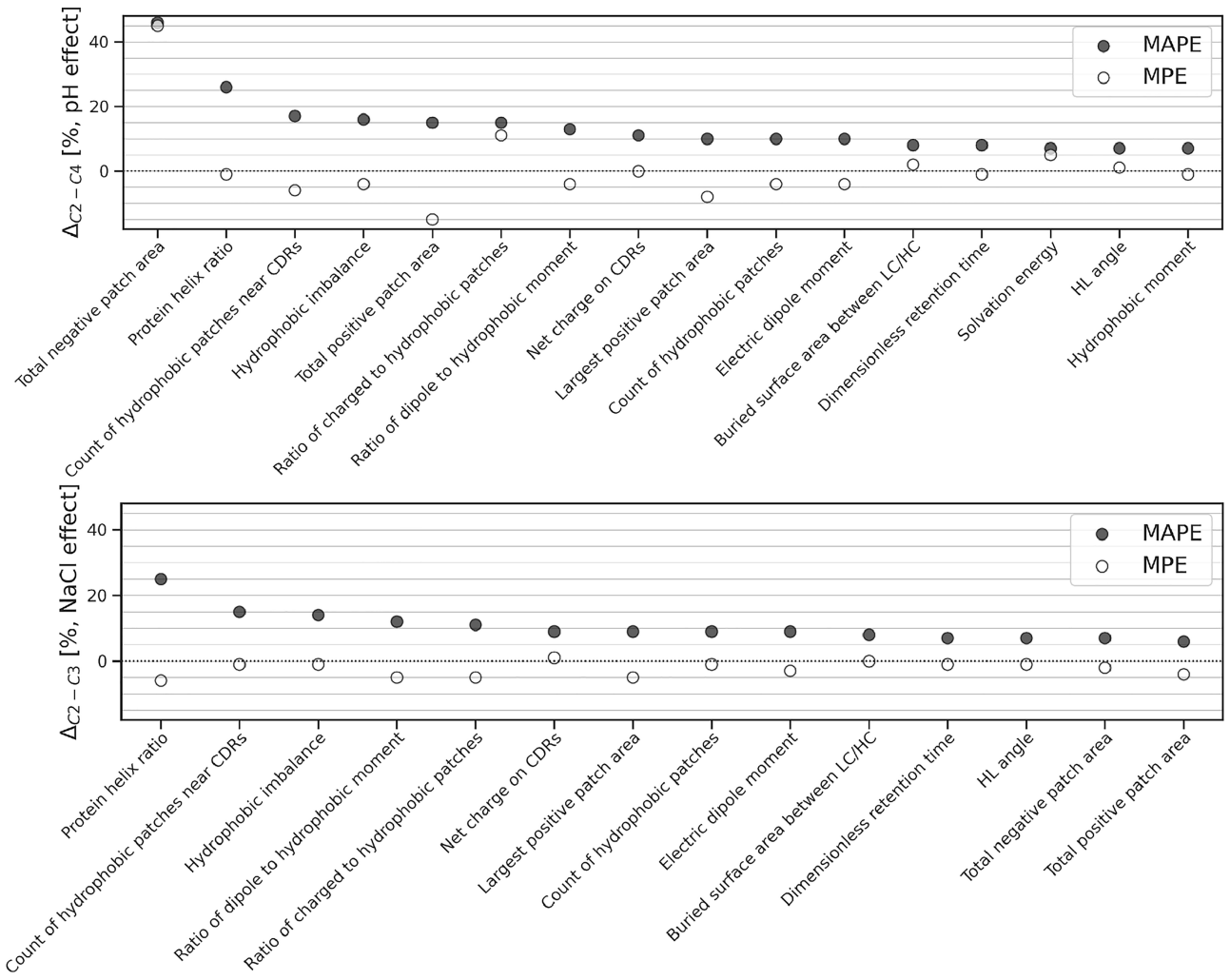

Figure 2. Effect of pH and NaCl on molecular descriptors obtained from the MD simulations. (Top) pH effect was obtained from the percentage change between C2 and C4 (no NaCl present). (Bottom) NaCl effect was instead retrieved from the percentage change between C2 and C3 (pH fixed at 6.0). The mean percentage error (MPE) and mean absolute percentage error (MAPE) were calculated through eq 2 as averages along all Fv regions (complete list in Table S5 and plot in Figure S17). Descriptors with a MAPE higher than 5% are reported.

previous simulations observed no significant differences among domain orientations in Fv, scFv, or Fabs.[66] Alternatively, this difference can be attributed to potential crystal packing effects in the homology model template with fewer exposed hydrophobic residues as to minimize contact with the aqueous environment.[60,67,68]

Geometric differences in the LC−HC interface arrangements were also observed, with systematic ∼8% longer distances between the two chains after the simulations ("dc distance" in Table S4) and an overall ∼4% decrease in torsion between the two variable domains ("HL angle", MAPE ∼9%).

Salt Presence and pH Affect the Surface Properties of Antibody Variable Regions. Solution conditions such as ionic strength and pH affect protein physicochemical properties, as reported by several studies.[69−72] A comparison between distributions obtained from MD simulations in different solution conditions illustrates that several molecular descriptors significantly change with NaCl concentration and pH (Figure 2 and Table S5). While positive patches systematically increase, on average, by 15% between pH 6.0 and pH 3.5, there is a larger systematic decrease in negative patches of 46%. These changes are driven by the protonation states of amino acids with charged side chains such as histidine, aspartate, and glutamate. This asymmetric change results in a total decrease in charged patches by 10% at low pH. As expected from previous experiments,[73−75] low pH increases the size as well as the number of hydrophobic patches (MAPE = 10% and MPE = −4% for the count of hydrophobic patches; MAPE = 17%, MPE = −6% for the count of hydrophobic patches near CDRs). The low pH promotes larger hydrophobic patches because of the decrease in total charged patches, which in turn triggers a more compact and favorable reorganization of hydrophobic residues. Taken together, the two charged and hydrophobic patch modulations cause a decrease in patch ratio (PR) by 11% on average. The effect of ions on charged patches is less evident (MAPE <7%) but still supports the formation of larger patches in the presence of NaCl. The hydrophobic properties of the Fv regions also change upon addition of NaCl (e.g., MAPE of 10 and 17% for count of hydrophobic patches for the whole Fv or near CDRs, respectively); however, the change is associated with only certain antibodies and is not generally observed for all antibodies (MPE ∼−1%).

Changes in NaCl concentration and pH did not cause significant changes in the structural arrangement of the Fv regions. For instance, the radius of gyration remains constant,

https://doi.org/10.1021/acs.molpharmaceut.2c00838
Mol. Pharmaceutics 2023, 20, 1096−1111

whereas $BSA_{VL:VH}$ and LC/HC torsion angles decrease only slightly upon lowering the pH.

Ion Interaction with the Fv Regions of Certain Market-Stage Antibodies Impacts Their Conformational Stabilities. Apart from being intrinsically encoded in the protein sequence and structure, the physicochemical behavior of mAbs can also depend on the extrinsic characteristics such as the type and concentration of excipients, co-solutes, and buffer in the antibody formulations.[70,76−78] Besides analyzing the effect of composition on specific molecular descriptors, we analyzed the MD simulations to understand the impact of specific ion interactions on the overall Fv conformational stability. Radial distribution functions, $g(r)$, were extracted between ions (Na^+ or Cl^-) and the center of mass of the Fv regions. No strong preferential binding to ions is observed for most of the antibodies. However, large peaks with values exceeding $g(r) > 4$ can be observed for specific antibodies (pertuzumab, polatuzumab, daclizumab, rituximab, and trastuzumab), pointing to a significant ion: protein interaction in the order of −0.5 to −1.5 kcal/mol for these antibodies (Figure 3A,B and Figure S18).

Most ion interactions with the Fv regions occur through chloride rather than sodium ions. This observation agrees with the Hofmeister series, which favor protein interactions with anions over cations,[79] and can be rationalized on the basis of the usually positive total charge on the Fv regions, determined by pI values being usually higher than the solution pH (the average structure-based pI is ∼7.8 ± 1.4 for all 91 Fvs), which increase the chance for electrostatic interaction with anions.[80] Chloride has a chaotropic character having a weak hydration shell that favors interactions with the protein surface, whereas sodium is a kosmotropic species that prefers interactions with water.

The conformational stability of the Fv regions was qualitatively assessed using the RMSD averaged along the last 20 ns of the trajectories.[81] The distributions of the RMSD were plotted by splitting the histograms according to the presence of sodium chloride in the drug formulation, as retrieved from the FDA package insert (Figure 3C, Table S1, 41 out of the 89 mAb formulations contained sodium or chloride ions). If the presence of NaCl does not affect the stability of the antibody, a similar RMSD distribution between the two sides of the violin plot is expected since there should be statistically no difference between the two groups of proteins simulated at one specific condition. Interestingly, the RMSD distributions obtained for the simulation conducted without NaCl (particularly C2, pH 6 without salt added) showed higher RMSD values for mAbs whose drug product formulations contained NaCl. This observation shows that the presence of NaCl can conformationally stabilize or destabilize certain mAbs.

To explore this hypothesis, the melting temperature (T_m) for 38 expressed antibodies was experimentally measured by thermal stability analysis at conditions comparable to C2 and C3 (complete list in Table S2 and thermal stability profiles in Figure S19). Even though the presence of NaCl decreased the T_m of ∼75% of the measured mAbs (28 of the 38 mAbs used for T_m evaluation), no general correlation between the change of T_m and the change in RMSD between conditions C2 and C3 was observed. However, a closer look at certain antibodies with strong ion interactions as indicated by the g(r)s in Figure 3 reveals that there is a correspondence between the change in melting temperature between C2 and C3 conditions and the structural fluctuation of the Fv region. For daclizumab and polatuzumab, an increase in T_m with the presence of NaCl (+1.4 and +0.7 °C) coincides with a decrease in RMSD (−0.8 and −0.4 Å, respectively). For pertuzumab, rituximab, and trastuzumab, the presence of ions causes a decrease in the melting temperature (−1.7, −3.0, and −1.6 °C) with a corresponding increase in RMSD (+0.1, +0.5, and +0.8 Å, respectively). In all cases, the ion pocket localizes within the cavity formed among all CDRs in HC and L3, with ions coordinated by acidic or basic residues.

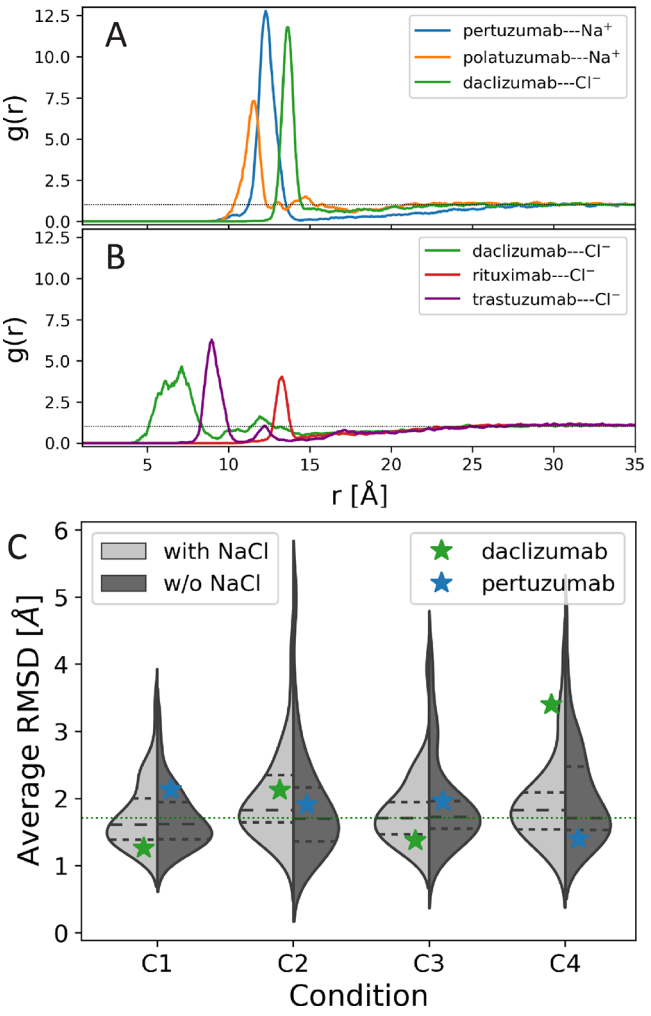

Figure 3. Radial distribution function, $g(r)$, between Na^+ or Cl^- and the center of mass of the Fv regions at condition C1 (A, pH 7.4 and 137 mM NaCl) and C3 (B, pH 6.0 and 150 mM NaCl) for the antibodies showing the strongest ion interaction (peak in $g(r)$ higher than 4). The horizontal dotted line indicates the $g(r)$ reaching the value of 1 at long distances. (C) The RMSD averaged for the last 20 ns of each trajectory is reported splitting the distribution according to the presence (light gray) or absence (dark gray) of NaCl in the drug product formulation extracted from the FDA (Food and Drug Administration) package insert. Values for daclizumab (green stars) and pertuzumab (blue stars) are indicated explicitly, and the marker position with respect to the side of the distribution indicates whether the antibody contains NaCl in the drug formulation.

Removal of Chloride Triggers Large Structural Fluctuations in Daclizumab. As an example of the effect that ions can have on certain antibodies, we report a detailed discussion on the molecular origins of the ion-induced conformational stabilization of daclizumab, a biotherapeutic drug approved for the treatment of relapsing forms of multiple sclerosis but withdrawn from the market in 2018.[82,83] From the

https://doi.org/10.1021/acs.molpharmaceut.2c00838
Mol. Pharmaceutics 2023, 20, 1096−1111

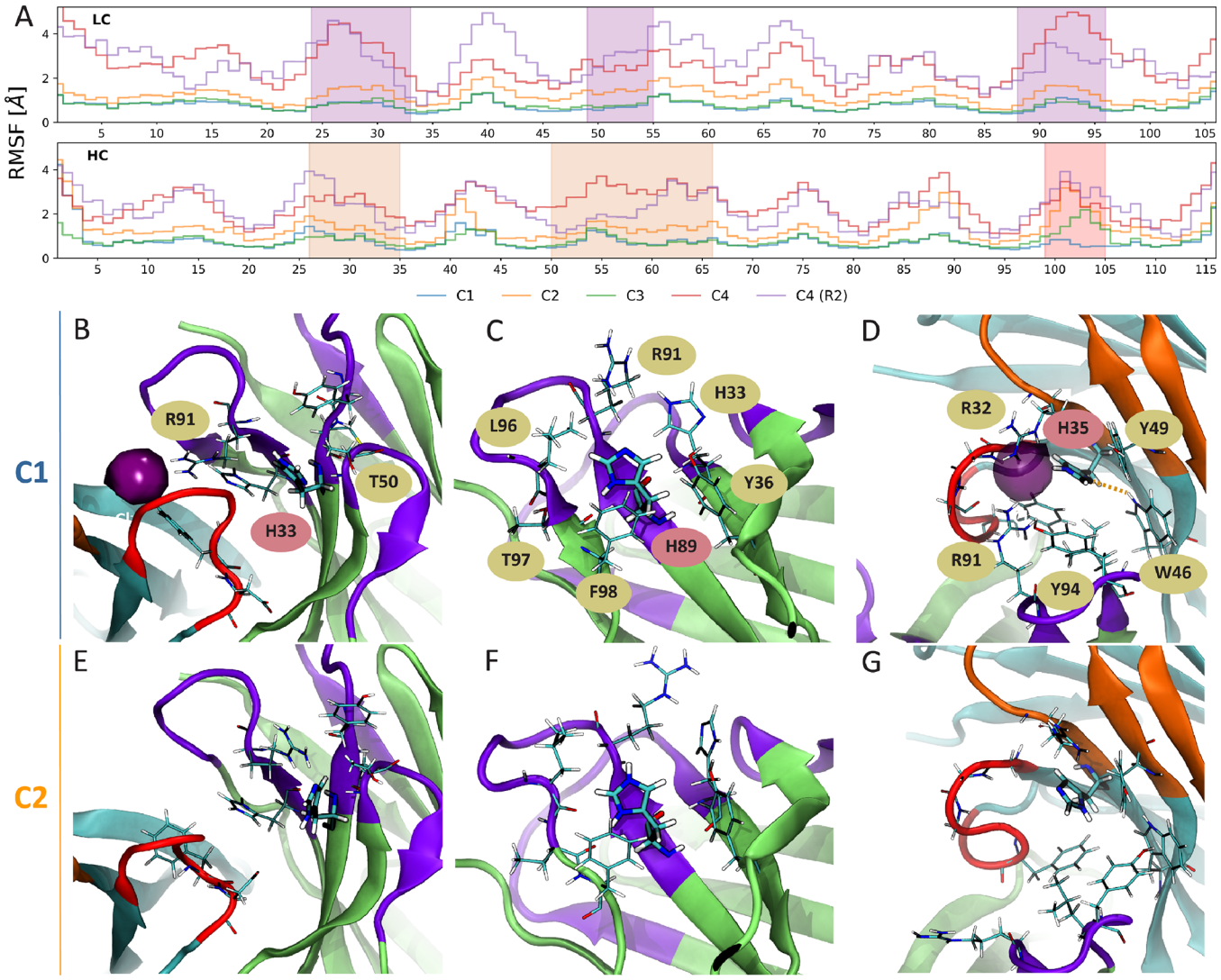

Figure 4. (A) RMSF for the daclizumab Fv region at different conditions (C1: blue, C2: orange, C3: green, C4: red, including one additional replica at C4 in purple). The shaded areas highlight the CDRs (L1−3: purple, H1−2: orange, and H3: red). Snapshots showing the last frame of daclizumab simulation at (B−D) C1 (pH 7.4, 137 mM NaCl) and (E−G) C2 (pH 6.0, no NaCl) with (B, E) H33, (C, F) H89 in LC, and (D, G) H35 in HC highlighted. The purple density shows the chloride occupancy at an isovalue of 0.04. Neighboring residues surrounding the histidine residues are visualized.

MD simulations, its Fv region undergoes large structural rearrangements in C2 and C4, with the result being reproducible (Figure 4A). The average RMSF is ∼0.8 Å in C1 (pH 7.4, 137 mM NaCl) and C3 (pH 6.0, 150 mM NaCl) but increases to 1.3 and 2.5 Å in C2 (pH 6.0, and no added NaCl) and C4 (pH 3.5 and no added NaCl). An extensive network of interactions is responsible for the ion sensitivity (Figure 4B−G and Figures S20 and S21). The changes in NaCl concentration and pH induce different protonation states for three histidine (His 33 & H89 in LC and His 35 in HC (CCG annotation reported), all within CDRs) and four glutamate residues (Glu 70 in LC and Glu 72, 80, and 87 in HC) in the Fv region. The protonation of glutamates at pH 3.5 reduces their H-bond acceptor capability but only has a minor effect on the stability of the Fv region because these glutamates are far from the LC−HC interface. On the other hand, each histidine residue is located at the interface between the VH and VL domains. Strikingly, a stable chloride pocket is formed between H1, H3, and L3 loops at conditions C1 and C3 (Figure 4D and Figure S21G). In this pocket, His 35 and Arg 32 in HC, Arg 91 in LC, and backbone amides from a few HC residues concertedly coordinate a chloride, with the anion occupying the pocket for 77% and 47% of the simulation time in C1 and C3, respectively. In addition, His 35 forms a H-bond with Trp 46 in HC, which stabilizes the folding of the L1 loop and the side-chain orientation of His 35. In the absence of NaCl at conditions C2 and C4, the chloride ion pocket is missing and interchain coordination is disrupted, with a detrimental effect on the V_H:V_L interface and H3 loop conformational stability (Figure 4E).

The other two histidine residues (His 33 and 89 in LC) also participate in this pH- and ion-sensitive interplay. For His 33 in LC, a stable interaction switches from backbone amide of Thr 50 toward the Arg 91 side chain, reducing the possibility for the latter to stabilize the anion binding pocket upon changing the environment from C1 to C2 (Figure 4B,E). Less dramatic changes are observed in the case of His 89 in the light chain, where the partially buried histidine becomes more solvent-exposed upon full protonation.

.

https://doi.org/10.1021/acs.molpharmaceut.2c00838
Mol. Pharmaceutics 2023, 20, 1096−1111

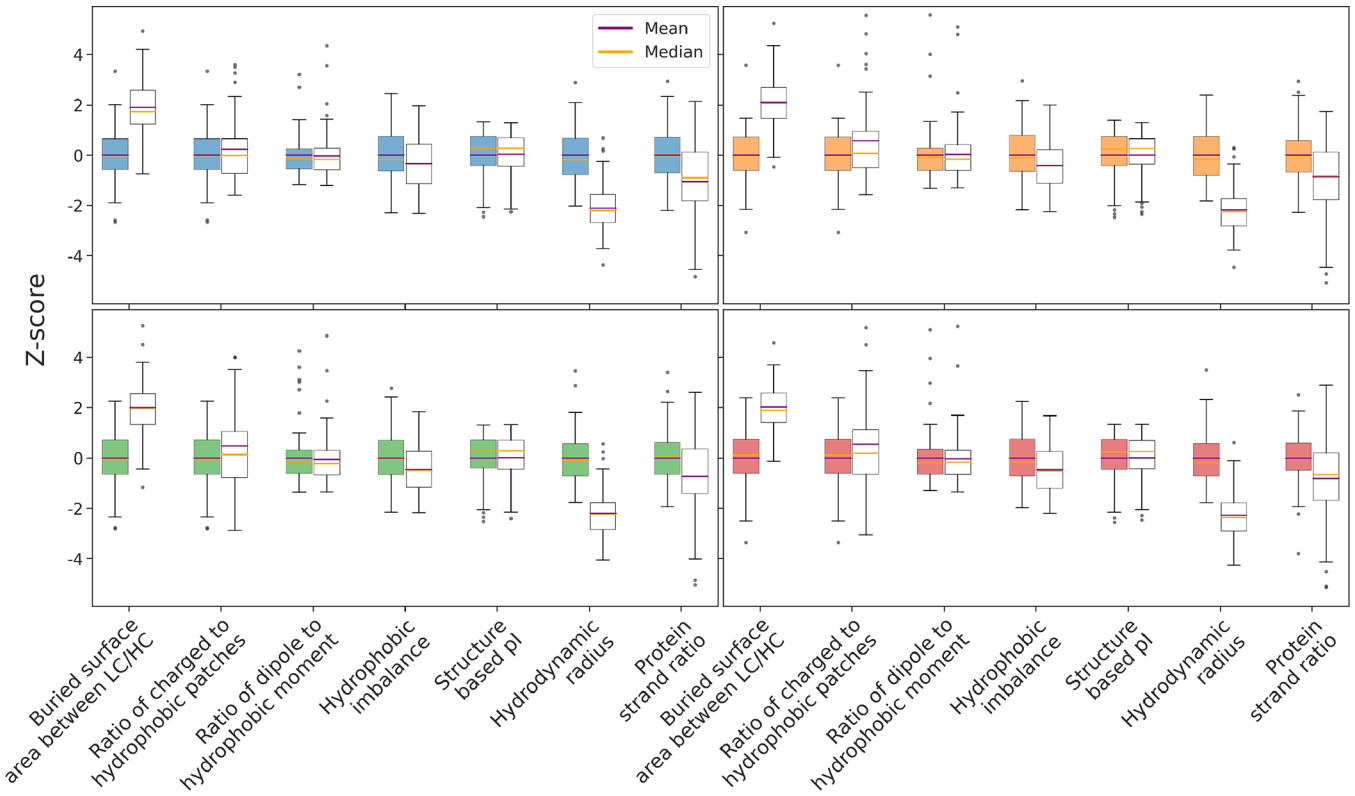

Figure 5. Intrinsic physicochemical profile of market-stage therapeutic Fvs showing the distribution of *Z*-scores for all seven descriptors and for static (white boxes) and simulated (colored boxes) systems at the four simulated conditions. The purple and orange bars represent the mean and median of the distribution, respectively. Outliers with *Z*-scores higher/lower than 6/−6 (1 for MD-based and 13 for static-based box plots) are not shown.

Table 2. Means, Standard Deviations, and Ranges (in Parentheses) for Seven Nonredundant Descriptors Obtained from the MD Simulations in Four Conditions

descriptor	C1: pH = 7.4 [NaCl] = 137 mM	C2: pH = 6.0	C3: pH = 6.0 [NaCl] = 150 mM	C4: pH = 3.5
buried surface area between LC/HC [Å^2]	671 ± 81 (456−941)	654 ± 82 (405−944)	653 ± 82 (425−835)	638 ± 93 (329−858)
ratio of charged to hydrophobic patches (RP)	2.0 ± 0.7 (0.9−5.4)	1.9 ± 0.7 (0.9−5.5)	2.0 ± 0.7 (1.0−5.2)	1.7 ± 0.5 (0.8−3.7)
ratio of dipole to hydrophobic moment [*D*] (RM)	1.2 ± 0.9 (0.2−6.7)	1.1 ± 0.7 (0.1−5.2)	1.2 ± 0.8 (0.1−4.4)	1.1 ± 0.7 (0.2−4.9)
hydrophobic imbalance (HI)	1.1 ± 0.4 (0.2−2.0)	1.1 ± 0.4 (0.3−2.2)	1.1 ± 0.4 (0.3−2.2)	1.1 ± 0.4 (0.3−2.0)
structure-based pI	7.7 ± 1.4 (4.3−9.6)	7.8 ± 1.4 (4.4−9.7)	7.8 ± 1.4 (4.3−9.6)	7.8 ± 1.4 (4.4−9.6)
hydrodynamic radius [Å] (HR)	23.6 ± 0.3 (23.0−24.5)	23.7 ± 0.3 (23.1−24.4)	23.7 ± 0.3 (23.2−24.7)	23.7 ± 0.3 (23.2−24.8)
protein strand ratio [%] (PS)	48.2 ± 1.9 (44.0−53.8)	48.0 ± 2.0 (43.4−53.9)	47.9 ± 2.0 (44.0−54.6)	48.1 ± 2.0 (40.4−53.2)

Intrinsic Physicochemical Profile for Biotherapeutics Can Be Improved by Using Conformational Ensembles of the Fv Regions. In the previous sections, we have shown how molecular descriptors and conformational stability of antibodies can be affected by the inclusion of conformational sampling and the use of different solution conditions. Envisioning an improvement in the accuracy of predictive models by embedding MD, we have built an intrinsic physicochemical profile for using the 91 Fv portions from 89 biotherapeutics with the molecular descriptors averaged along the simulation trajectories. The high-variance descriptors were clustered as described in the Materials and Methods section, and hierarchical dendrograms were used to identify non-redundant descriptors (Figures S5−S14). For all simulated conditions, seven unique and orthogonal descriptors were selected (Figure 5): $BSA_{VL:VH}$, RP, RM, HI, structure-based pI, hydrodynamic radius (HR), and protein strand ratio (PS). The first five of these descriptors also formed the intrinsic physicochemical profile built by Ahmed et al.[30] using the energy-minimized homology-based structural models of 77 biotherapeutics. $BSA_{VL:VH}$ quantifies the contact area between the V_L and V_H domains of an Fv region. Higher values are associated with increased protein stability, as can be seen from its average value rising from ∼640 to ∼670 Å going from pH 3.5 to 7.4 (Table 2). Better interface stability between the two domains can translate even to higher antigen affinity. The presence of significantly large charged and hydrophobic surface patches can affect the solution behavior (aggregation, viscosity) and immunogenicity of biologic molecules.[84−89] The RP was introduced to track the change in such surface patches using a single value.[30] Values out of typical ranges on both sides of the distribution can be potentially associated with greater development risks. Among the simulated conditions, low pH (C4) causes RP to significantly reduce (Table 2), highlighting that this pH poses greater challenges for controlling protein stability. RM equals the ratio between two fundamental quantities, the electric dipole moment, and the

https://doi.org/10.1021/acs.molpharmaceut.2c00838
Mol. Pharmaceutics 2023, 20, 1096−1111

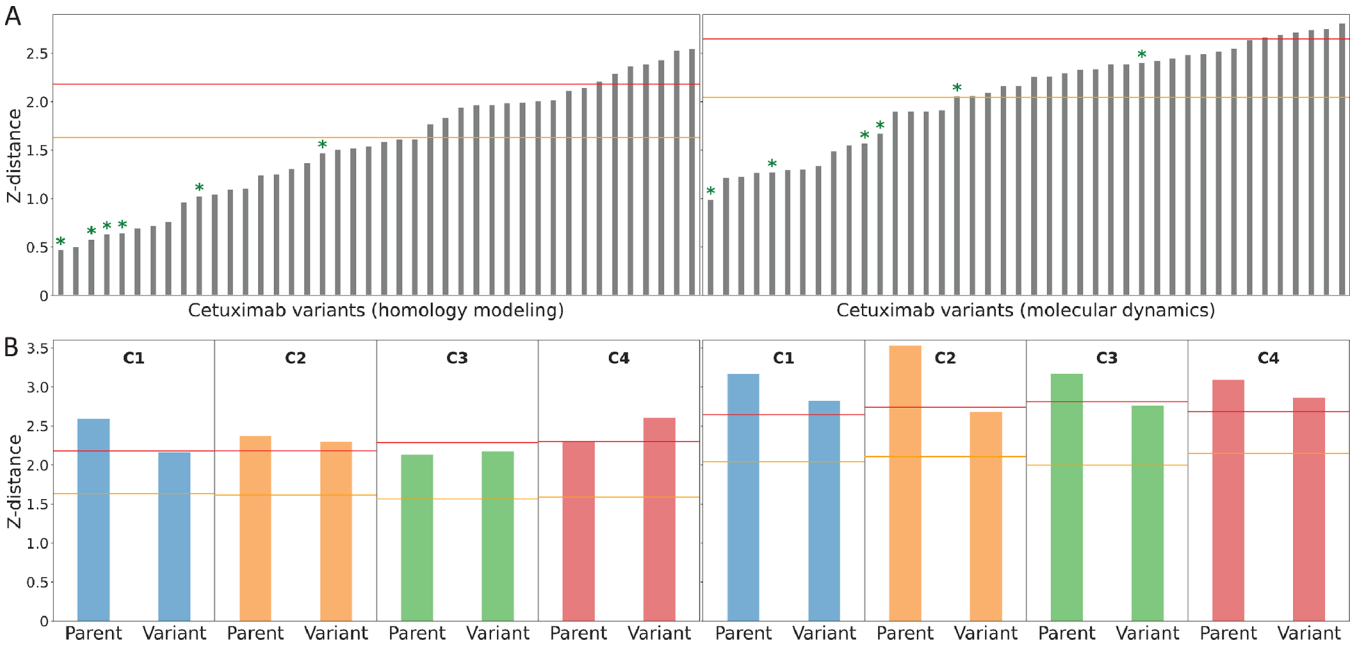

Figure 6. Candidates ranking according to *Z*-distance obtained from homology models (left) or including dynamics through MD simulations (right). (A) A set of cetuximab variants modeled at the C1 condition was used as a first test case.[93] Variants with melting temperatures higher than 80 °C are highlighted with a green asterisk. The T_m and DENIS values are reported in Table S6. (B) A parent/variant (single mutation) pair, with the variant having a threefold increased product titer, reduced level of aggregates, and fragments after downstream process purification and enhanced colloidal stability, was used as a second test case.[94] DENIS was applied in all four simulation conditions (C1−C4). Orange and red horizontal lines indicate 33 and 67% population of the reference 91 Fv region dataset at the specific simulation condition.

hydrophobic moment, characterizing the distribution of charged and hydrophobic residues in the biologic molecule, respectively. Together, they can report on protein−protein and protein−solvent interactions through polar and non-polar residues. The HI, previously introduced,[63] and the structure-based isoelectric point (pI, i.e., pH at which a protein carries no net electrical charge) do not show large changes in the different conditions. However, they are also crucial for determining the solution behavior of biotherapeutics in terms of colloidal stability, aggregation, and pharmacokinetics.[63,90−92] Two additional descriptors, namely, HR and PS, were identified by the MD simulations as characterizing antibodies in a unique and orthogonal way. HR is defined through the size and mass of a macromolecule and is connected to its diffusivity in solution. The PS refers to the amount of β-sheet content in the protein and is indicative of folding stability associated with a secondary structure. Both HR and PS relate to the conformation stabilities and flexibilities of the variable regions.

Z-scores (eq 3) of the seven descriptors obtained from the MD simulations were compared to the *Z*-scores of the 91 initial homology-based models. While the MD profiles show at all conditions only one outlier, defined as a datapoint with *Z*-scores higher/lower than 6/−6, there are 13 outliers for profiles from static models. A higher number of outliers are also observed in the *Z*-distance space at different conditions (Figure S22). Moreover, the standard deviation of *Z*-distance is systematically smaller after the simulations (from 1.3−1.5 using homology models to 0.8−0.9 using MD simulations). Therefore, the physicochemical properties obtained from MD simulations converge better than those from the static models. Given the distribution of the seven orthogonal descriptors after MD simulations, we noticed no significant changes for five of them when comparing conditions C1−C4 (Table 2). However, $BSA_{VL:VH}$ and RP show clear changes that are particularly pronounced at low pH (C4). Consequently, these two descriptors represent the key features of the MD-based physicochemical profile that can discriminate between antibody candidates in different environment conditions.

Altogether, MD simulations improve the in silico derived intrinsic physicochemical profiles by (a) increasing the accuracy and precision of the computed properties, (b) bringing in two additional non-redundant descriptors that provide insights into dynamic behaviors of the Fvs regions, and (c) considering environmental conditions experienced by biotherapeutics under physiological as well as different manufacturing and formulation processing conditions. These more stringent profiles can potentially help better guide the developability assessments of leads selected for optimization.

Applying the MD-Enhanced Intrinsic Physicochemical Profile to Biotherapeutic Case Studies. The greatest potential of the intrinsic physicochemical profile of market-stage biotherapeutics is the selection and optimization of lead candidates for discovery and development. To evaluate the performance of the intrinsic physicochemical profile and the benefits introduced by embedding the protein dynamics, the MD-based DENIS was tested relative to the homology modeling-based one[30] on a series of cetuximab variants that have been optimized for thermal stability.[93] Although thermal stability is not the only parameter determining biotherapeutics developability, it is generally related to a lower unfolding propensity,[12] a lower risk for aggregation,[27,95] and better expression titer.[9,96] Both DENIS approaches are able to rank the variants with the highest thermal stability as having a low *Z*-distance (always within 67% of the antibodies, Figure 6A). However, homology modeling-based DENIS is less selective. It lists 24 variants within 33% of the mAb population instead of 16 identified by the MD-based one. Moreover, the MD-based profile classifies the G2 VH/G2 Vκ as the best candidate, which

https://doi.org/10.1021/acs.molpharmaceut.2c00838
Mol. Pharmaceutics 2023, 20, 1096−1111

also exhibited the highest thermal stability among all variants in the dataset with a T_m of 82.5 °C.

In a second case, a difficult-to-develop mAb (a G6 parent antibody) that binds vascular endothelial growth factor (VEGF, Protein Data Bank (PDB) entry 2FJF)[97] was evaluated via DENIS in all four conditions (C1−C4, Figure 6B) relative to an optimized variant that showed significantly improved CMC (Chemistry, Manufacturing, and Control) characteristics after substituting a single amino acid (S52R in LC).[94] During experimental evaluation, the variant showed a threefold increased product titer, reduced level of aggregates and fragmentation during the downstream purification, and enhanced colloidal stability, while maintaining potency similar to the parent antibody.[94] Improved characteristics for the variant were also demonstrated at low pH applied during acidic treatment. HM-based DENIS was able to rank the parent/variant correctly only in conditions C1 and C2, while MD-based DENIS systematically favored the variant in all simulation conditions. Contrary to the MD-based counterpart, the original HM-based model indicated opposite rankings at C2 and C3 (without and with NaCl), probably due to differences in the homology models of parent and variant obtained at the two conditions. The MD-based DENIS profile sensitively predicted the improved developability of the variant even if the sequence only differs at one position from the parental mAb.

As the final case study, the NIST (National Institute for Standards and Technology) sample reference monoclonal antibody (NIST mAb)[98] was analyzed using the method developed in this work, even though this antibody is not a biotherapeutic drug candidate or product. The NIST mAb has been previously characterized for its biophysical properties using a variety of experiments,[90] which makes this antibody another useful resource for us. The experimental data available on this mAb corresponds to the conditions C2 and C3 (pH 6 without and with added salt, respectively). In these two conditions, all the seven physicochemical descriptors computed from MD trajectories of NIST mAb's variable region fall within the ranges observed for 91 Fvs from the market-stage biotherapeutics (see Table S7 and Table 2) and therefore the MD-based DENIS shows small Z-distance values for this antibody (Z-distance = 1.90 for C2 and 1.86 for C3). The values of Z-distance for the NIST mAb in the other two conditions C1 (1.78) and C4 (1.51) are also small, and all the seven descriptors also fall within the ranges observed for the market-stage biotherapeutics for these conditions (see Table 2). Figure S23 compares the intrinsic physicochemical profile of NIST mAb with the 91 Fvs from the market-stage biotherapeutics in the C2 condition using the Z-score box plots. All the seven non-redundant physicochemical descriptors, except for the PS, fall within their respective boxes. PS shows higher Z-scores in the other three conditions also (Table S7). Additionally, Table S7 shows that the Z-scores for all seven descriptors in all four conditions vary from −0.78 to 1.62, showing thereby that physicochemical properties of the NIST mAb are similar to those of the market-stage biotherapeutics. These observations agree with results from the extended experimental characterizations of the developability of the NIST mAb reported in the literature.[99,100]

■ DISCUSSION

Solution behaviors of biotherapeutic macromolecules are determined by multiple factors, namely, their amino acid sequences, their molecular surface characteristics, and characteristics of their environmental conditions (e.g., formulation buffers, excipients, pH, ionic strengths, or surfactants). In this work, in silico physicochemical profiles for 91 Fv regions from 89 market-stage antibodies were built after simulations for hundreds of nanoseconds in four different conditions: physiological, formulation with or without added ions, and low pH hold. These solution environments are experienced by the biotherapeutic drug candidates at various stages of production, storage, and administration. These phenomenological profiles can provide valuable guidelines for developability assessments of biotherapeutic drug candidates, particularly during lead optimization. Our previous work on physicochemical profiling of the market-stage biotherapeutics was based on the energy-minimized homology models of 79 Fv regions from 77 biotherapeutics available in the market as of early 2020.[30] Here, we found for an updated list of 91 Fv regions from 89 biotherapeutics that the HM-based approach can be significantly improved by accounting for the protein conformational dynamics, which in turn enabled a more precise definition of intrinsic physicochemical profile for the market-stage antibody-based biotherapeutics. Inclusion of MD reveals additional descriptors that may be important for conformational stability of the variable regions. Hydrodynamic radius and PS are the two additional descriptors included in the MD-based DENIS to increase its selective power. The application of the new profiles to a parent/variant mAb pair clearly showed that the inclusion of protein dynamics provides a more robust ranking capability in all tested simulation conditions. The experimental data highlight a better developability for the variant at both low and high pH, which was correctly accounted for only by the MD-based profile. An early, fast, and efficient in silico screening by DENIS can assist in making data-informed decisions at important project milestones during lead optimization and selection of the final candidate for start of drug development.

There are several limitations to the applicability of the intrinsic physicochemical profiles derived solely from sequence and structural characteristics of the Fv regions of the market-stage antibodies. First, it must be stated that the profiles described in this work and also previously described ones are essentially phenomenological models.[26,28,30] They are not suitable for drawing any inferences about causal relationships rooted in the laws of physics and chemistry. That is, such models are inherently incapable of explaining why some biotherapeutic drug candidates can successfully navigate through different stages of drug product development, clinical pharmacology, safety and efficacy testing, regulatory approvals, and commercialization while several others cannot. Furthermore, these profiles cannot describe the mechanism of action or to infer a target-mediated toxicology effect of the biotherapeutic drug. Such drug characteristics rely on many other aspects that may not be accounted for by the intrinsic molecular properties of Fv regions. An extension of DENIS to Fabs and full-length models can potentially improve the applicability and accuracy of mAb rankings for standard IgG derivatives and multi-specific formats. Thereby, a modified set of physicochemical descriptors might be used to characterize full-length mAbs accurately. Even if the full exploration of a full-length mAbs' conformational space remains computationally daunting, a limited sampling can potentially still reveal interactions affecting its overall solution behavior.[65] The conditions considered in this work can be extended to other experimental scenarios experienced during manufacturing and storage. It should also be stated that use of MD-based intrinsic physicochemical profiles to assess the similarity of the drug candidates with the market-stage biotherapeutics is not practical

https://doi.org/10.1021/acs.molpharmaceut.2c00838
Mol. Pharmaceutics 2023, 20, 1096−1111

at the earliest stage of drug discovery, namely, hit selection, which involves high-throughput screening of potential binders obtained from antibody generation campaigns. Homology-based intrinsic physicochemical profiles at such stages can still be successfully used to identify promising hits for further experimental studies.

The analyses of the MD simulations of the market-stage antibodies revealed that pH and ions can have a strong impact on the structure and the physicochemical properties of the Fv regions. Lowering the pH can potentially cause larger structural fluctuations and an asymmetric change in charged patches. Together with an increase in hydrophobic patches, self-association is then facilitated, explaining the tendency of certain mAbs to aggregate at low pH.[73,101]

The effect of ions on molecular surface patches is smaller than that of pH but not negligible. Therefore, the choice of salts can potentially modulate an antibody's solution behavior, with significant implications for downstream processing and pH-buffer formulation screening. Specific interactions of ions with solvent-exposed residues on the molecular surface can affect antibody structural organization with both stabilizing and perturbing roles. This is consistent with the knowledge that ions can directly bind proteins and affect their solution behaviors, as in the case of chloride binding to enzymes or transporters and influencing their spatial arrangement and function.[102] The analyses shown here highlight important but opposing roles of ionic strength for conformational stability of API (active pharmaceutical ingredient) in formulation. The case study of daclizumab revealed the presence of the chloride ion pocket in the middle of CDRs, which explains how the absence of chloride anion in solution triggers large fluctuations in its Fv region. Note that the final drug formulation of daclizumab contains NaCl as per information available via Package inserts. From the Wyman linkage theory,[103] ions can interact with charged side chains on the surface of the antibody and lead to a stabilization of the protein native state.[104] On the other hand, ions binding more strongly to non-native protein states will destabilize the folding and possibly promote subsequent protein aggregation.

A similar computational approach, as discussed herein, can be used to build models that can predict the stability of a drug in different formulations with changes in buffer composition, excipients, or co-solutes. Development of such tools is nowadays computationally feasible and can have a favorable impact on the speed and cost of biologic drug development. The advantage of using computational approaches such as MD simulations relies on the fact that the stability of a protein can be assessed by simply analyzing the data without any prior assumption on the effect of specific ions or pH. However, there are only scarce examples of application and validation in this direction and more work is required to build standardized procedures and protocols.

■ ASSOCIATED CONTENT

Data Availability Statement

We have uploaded in Zenodo (10.5281/zenodo.7365277) the following SI materials: (1) *fasta* file containing all 91 sequences of reference biotherapeutics, (2) all PDB files of the homology models at all simulated conditions, and (3) Excel files reporting all 125 calculated descriptors in homology models and averaged along the simulations.

Supporting Information

The Supporting Information is available free of charge at https://pubs.acs.org/doi/10.1021/acs.molpharmaceut.2c00838.

Generic names, molecular formats, heavy and light chain isotypes, and formulations (PDF)

Publicly available information on 89 market-stage biotherapeutics studied in this work (XLSX)

■ AUTHOR INFORMATION

Corresponding Authors

Sandeep Kumar − *Biotherapeutics Discovery & In silico Team, Boehringer Ingelheim Pharmaceuticals Inc., Ridgefield, Connecticut 06877, United States;* orcid.org/0000-0003-2840-6398; Email: Sandeep_2.Kumar@boehringer-ingelheim.com

Joschka Bauer − *Early Stage Pharmaceutical Development, Pharmaceutical Development Biologicals & In silico Team, Boehringer Ingelheim International GmbH & Co. KG, Biberach/Riss 88397, Germany*; Email: Joschka.Bauer@boehringer-ingelheim.com

Authors

Giuseppe Licari − *Early Stage Pharmaceutical Development, Pharmaceutical Development Biologicals & In silico Team, Boehringer Ingelheim International GmbH & Co. KG, Biberach/Riss 88397, Germany;* orcid.org/0000-0002-8490-7536

Kyle P. Martin − *Biotherapeutics Discovery & In silico Team, Boehringer Ingelheim Pharmaceuticals Inc., Ridgefield, Connecticut 06877, United States*

Maureen Crames − *Biotherapeutics Discovery & In silico Team, Boehringer Ingelheim Pharmaceuticals Inc., Ridgefield, Connecticut 06877, United States*

Joseph Mozdzierz − *Biotherapeutics Discovery & In silico Team, Boehringer Ingelheim Pharmaceuticals Inc., Ridgefield, Connecticut 06877, United States*

Michael S. Marlow − *Biotherapeutics Discovery & In silico Team, Boehringer Ingelheim Pharmaceuticals Inc., Ridgefield, Connecticut 06877, United States*

Anne R. Karow-Zwick − *Early Stage Pharmaceutical Development, Pharmaceutical Development Biologicals & In silico Team, Boehringer Ingelheim International GmbH & Co. KG, Biberach/Riss 88397, Germany*

Complete contact information is available at: https://pubs.acs.org/10.1021/acs.molpharmaceut.2c00838

Author Contributions

G.L., conceptualization, methodology, formal analysis, writing—original draft; K.P.M., resources, writing—review and editing; M.C., resources, writing—review and editing; J.M., resources, writing—review and editing; M.M., resources, writing—review and editing; A.K.-Z., funding acquisition, writing—review and editing; S.K., conceptualization, writing—review and editing; and J.B., conceptualization, writing—review and editing.

Notes

The authors declare the following competing financial interest(s): The authors were employees of Boehringer Ingelheim Pharma GmbH & Co. KG during the project.

https://doi.org/10.1021/acs.molpharmaceut.2c00838
Mol. Pharmaceutics 2023, 20, 1096−1111

■ ACKNOWLEDGMENTS

This research was supported by Boehringer Ingelheim Pharma GmbH & Co KG. We gratefully acknowledge Jens Smiatek, Mark Schuette, and the whole In Silico Team at Boehringer Ingelheim for excellent discussions.

■ ABBREVIATIONS

mAb, monoclonal antibody; HM, homology model; SAP, spatial aggregation propensity; CDR, complementary-determining region; TAP, therapeutic antibody profiler; LC, light chain; HC, heavy chain; Fv, antibody variable region; Fab, fragment antigen-binding; V_L, variable region in LC; V_H, variable region in HC; HL, heavy/light; MD, molecular dynamics; DENIS, developability navigator in silico; WHO, World Health Organization; TABS, Therapeutic Antibody Database; IMGT, International ImMunoGeneTics Information system; FDA, Food and Drug Administration; MOE, molecular operating environment; EHT, extended Hückel theory; CCG, Chemical Computing Group; PME, particle mesh Ewald; RMSD, root mean square deviation; RMSF, root mean square fluctuation; MPE, mean percentage error; MAPE, mean absolute percentage error; $BSA_{VL:VH}$, buried surface area between V_L and V_H; pI, protein isoelectric point; RP, ratio of surface areas of positively and negatively charged patches to that of hydrophobic patches; RM, ratio of dipole moment to hydrophobic moment; HI, hydrophobic imbalance; HR, hydrodynamic radius; PS, protein strand ratio; T_m, protein melting temperature; API, active pharmaceutical ingredient.

■ REFERENCES

(1) Kumar, D.; Gauthami, S.; Bayry, J.; Kaveri, S. V.; Hegde, N. R. Antibody Therapy: From Diphtheria to Cancer, COVID-19, and Beyond. *Monoclonal Antibodies Immunodiagn. Immunother.* **2021**, *40*, 36−49.

(2) Zhong, X.; D'Antona, A. M. Recent Advances in the Molecular Design and Applications of Multispecific Biotherapeutics. *Antibodies* **2021**, *10*, 13.

(3) Kaplon, H.; Reichert, J. M. Antibodies to Watch in 2021. *mAbs* **2021**, *13*, 1860476.

(4) Pammolli, F.; Righetto, L.; Abrignani, S.; Pani, L.; Pelicci, P. G.; Rabosio, E. The Endless Frontier? The Recent Increase of R&D Productivity in Pharmaceuticals. *J. Transl. Med.* **2020**, *18*, 162.

(5) Smietana, K.; Siatkowski, M.; Møller, M. Trends in Clinical Success Rates. *Nat. Rev. Drug Discovery* **2016**, *15*, 379−380.

(6) Pérez, A.-M. W.; Lorenzen, N.; Vendruscolo, M.; Sormanni, P. Therapeutic Antibodies, Methods and Protocols. *Methods Mol. Biol.* **2022**, *2313*, 57−113.

(7) Sawant, M. S.; Streu, C. N.; Wu, L.; Tessier, P. M. Toward Drug-Like Multispecific Antibodies by Design. *Int. J. Mol. Sci.* **2020**, *21*, 7496.

(8) Jarasch, A.; Koll, H.; Regula, J. T.; Bader, M.; Papadimitriou, A.; Kettenberger, H. Developability Assessment During the Selection of Novel Therapeutic Antibodies. *J. Pharm. Sci.* **2015**, *104*, 1885−1898.

(9) Jain, T.; Sun, T.; Durand, S.; Hall, A.; Houston, N. R.; Nett, J. H.; Sharkey, B.; Bobrowicz, B.; Caffry, I.; Yu, Y.; Cao, Y.; Lynaugh, H.; Brown, M.; Baruah, H.; Gray, L. T.; Krauland, E. M.; Xu, Y.; Vásquez, M.; Wittrup, K. D. Biophysical Properties of the Clinical-Stage Antibody Landscape. *Proc. Natl. Acad. Sci.* **2017**, *114*, 944−949.

(10) Wang, Q.; Chen, Y.; Park, J.; Liu, X.; Hu, Y.; Wang, T.; McFarland, K.; Betenbaugh, M. J. Design and Production of Bispecific Antibodies. *Antibodies* **2019**, *8*, 43.

(11) Bailly, M.; Mieczkowski, C.; Juan, V.; Metwally, E.; Tomazela, D.; Baker, J.; Uchida, M.; Kofman, E.; Raoufi, F.; Motlagh, S.; Yu, Y.; Park, J.; Raghava, S.; Welsh, J.; Rauscher, M.; Raghunathan, G.; Hsieh, M.; Chen, Y.-L.; Nguyen, H. T.; Nguyen, N.; Cipriano, D.; Fayadat-Dilman, L. Predicting Antibody Developability Profiles Through Early Stage Discovery Screening. *mAbs* **2020**, *12*, 1743053.

(12) Xu, Y.; Wang, D.; Mason, B.; Rossomando, T.; Li, N.; Liu, D.; Cheung, J. K.; Xu, W.; Raghava, S.; Katiyar, A.; Nowak, C.; Xiang, T.; Dong, D. D.; Sun, J.; Beck, A.; Liu, H. Structure, Heterogeneity and Developability Assessment of Therapeutic Antibodies. *mAbs* **2019**, *11*, 1−264.

(13) Yang, R.; Jain, T.; Lynaugh, H.; Nobrega, R. P.; Lu, X.; Boland, T.; Burnina, I.; Sun, T.; Caffry, I.; Brown, M.; Zhi, X.; Lilov, A.; Xu, Y. Rapid Assessment of Oxidation via Middle-down LCMS Correlates with Methionine Side-Chain Solvent-Accessible Surface Area for 121 Clinical Stage Monoclonal Antibodies. *mAbs* **2017**, *9*, 646−653.

(14) Sharma, V. K.; Patapoff, T. W.; Kabakoff, B.; Pai, S.; Hilario, E.; Zhang, B.; Li, C.; Borisov, O.; Kelley, R. F.; Chorny, I.; Zhou, J. Z.; Dill, K. A.; Swartz, T. E. In Silico Selection of Therapeutic Antibodies for Development: Viscosity, Clearance, and Chemical Stability. *Proc. Natl. Acad. Sci.* **2014**, *111*, 18601−18606.

(15) Karlberg, M.; de Souza, J. V.; Fan, L.; Kizhedath, A.; Bronowska, A. K.; Glassey, J. QSAR Implementation for HIC Retention Time Prediction of MAbs Using Fab Structure: A Comparison between Structural Representations. *Int. J. Mol. Sci.* **2020**, *21*, 8037.

(16) Jetha, A.; Thorsteinson, N.; Jmeian, Y.; Jeganathan, A.; Giblin, P.; Fransson, J. Homology Modeling and Structure-Based Design Improve Hydrophobic Interaction Chromatography Behavior of Integrin Binding Antibodies. *mAbs* **2018**, *10*, 1−900.

(17) Agrawal, N. J.; Helk, B.; Kumar, S.; Mody, N.; Sathish, H. A.; Samra, H. S.; Buck, P. M.; Li, L.; Trout, B. L. Computational Tool for the Early Screening of Monoclonal Antibodies for Their Viscosities. *mAbs* **2016**, *8*, 43−48.

(18) Li, L.; Kumar, S.; Buck, P. M.; Burns, C.; Lavoie, J.; Singh, S. K.; Warne, N. W.; Nichols, P.; Luksha, N.; Boardman, D. Concentration Dependent Viscosity of Monoclonal Antibody Solutions: Explaining Experimental Behavior in Terms of Molecular Properties. *Pharm. Res.* **2014**, *31*, 3161−3178.

(19) Pérez, A.-M. W.; Sormanni, P.; Andersen, J. S.; Sakhnini, L. I.; Rodriguez-Leon, I.; Bjelke, J. R.; Gajhede, A. J.; Maria, L. D.; Otzen, D. E.; Vendruscolo, M.; Lorenzen, N. In Vitro and in Silico Assessment of the Developability of a Designed Monoclonal Antibody Library. *mAbs* **2019**, *11*, 388−400.

(20) Kant, R. V. D.; Durme, J. V.; Rousseau, F.; Schymkowitz, J. Protein Misfolding Diseases, Methods and Protocols. *Methods Mol. Biol. Clifton N. J.* **2018**, *1873*, 317−333.

(21) Chennamsetty, N.; Voynov, V.; Kayser, V.; Helk, B.; Trout, B. L. Prediction of Aggregation Prone Regions of Therapeutic Proteins. *J. Phys. Chem. B* **2010**, *114*, 6614−6624.

(22) Dostalek, M.; Prueksaritanont, T.; Kelley, R. F. Pharmacokinetic De-Risking Tools for Selection of Monoclonal Antibody Lead Candidates. *mAbs* **2017**, *9*, 756−766.

(23) Wang, J.; Iyer, S.; Fielder, P. J.; Davis, J. D.; Deng, R. Projecting Human Pharmacokinetics of Monoclonal Antibodies from Nonclinical Data: Comparative Evaluation of Prediction Approaches in Early Drug Development. *Biopharm. Drug Dispos.* **2016**, *37*, 51−65.

(24) Liang, S.; Zhang, C. Prediction of Immunogenicity for Humanized and Full Human Therapeutic Antibodies. *PLoS One* **2020**, *15*, No. e0238150.

(25) Walle, I. V.; Gansemans, Y.; Parren, P. W.; Stas, P.; Lasters, I. Immunogenicity Screening in Protein Drug Development. *Expert Opin. Biol. Th.* **2007**, *7*, 405−418.

(26) Lauer, T. M.; Agrawal, N. J.; Chennamsetty, N.; Egodage, K.; Helk, B.; Trout, B. L. Developability Index: A Rapid in Silico Tool for the Screening of Antibody Aggregation Propensity. *J. Pharm. Sci.* **2012**, *101*, 102−115.

(27) Chennamsetty, N.; Voynov, V.; Kayser, V.; Helk, B.; Trout, B. L. Design of Therapeutic Proteins with Enhanced Stability. *Proc. Natl. Acad. Sci.* **2009**, *106*, 11937−11942.

(28) Raybould, M. I. J.; Marks, C.; Krawczyk, K.; Taddese, B.; Nowak, J.; Lewis, A. P.; Bujotzek, A.; Shi, J.; Deane, C. M. Five Computational Developability Guidelines for Therapeutic Antibody Profiling. *Proc. Natl. Acad. Sci.* **2019**, *116*, 4025−4030.

(29) Thorsteinson, N.; Gunn, J. R.; Kelly, K.; Long, W.; Labute, P. Structure-Based Charge Calculations for Predicting Isoelectric Point, Viscosity, Clearance, and Profiling Antibody Therapeutics. *mAbs* **2021**, *13*, 1981805.
(30) Ahmed, L.; Gupta, P.; Martin, K. P.; Scheer, J. M.; Nixon, A. E.; Kumar, S. Intrinsic Physicochemical Profile of Marketed Antibody-Based Biotherapeutics. *Proc. Natl. Acad. Sci.* **2021**, *118*, No. e2020577118.
(31) Fernández-Quintero, M. L.; Georges, G.; Varga, J. M.; Liedl, K. R. Ensembles in Solution as a New Paradigm for Antibody Structure Prediction and Design. *mAbs* **2021**, *13*, 1923122.
(32) Fernández-Quintero, M. L.; Heiss, M. C.; Pomarici, N. D.; Math, B. A.; Liedl, K. R. Antibody CDR Loops as Ensembles in Solution vs. Canonical Clusters from X-Ray Structures. *mAbs* **2020**, *12*, 1744328.
(33) Lai, P.-K.; Fernando, A.; Cloutier, T. K.; Kingsbury, J. S.; Gokarn, Y.; Halloran, K. T.; Calero-Rubio, C.; Trout, B. L. Machine Learning Feature Selection for Predicting High Concentration Therapeutic Antibody Aggregation. *J. Pharm. Sci.* **2021**, *110*, 1583−1591.
(34) Cloutier, T. K.; Sudrik, C.; Mody, N.; Sathish, H. A.; Trout, B. L. Machine Learning Models of Antibody−Excipient Preferential Interactions for Use in Computational Formulation Design. *Mol. Pharmaceutics* **2020**, *17*, 3589−3599.
(35) Shmool, T. A.; Martin, L. K.; Bui-Le, L.; Moya-Ramirez, I.; Kotidis, P.; Matthews, R. P.; Venter, G. A.; Kontoravdi, C.; Polizzi, K. M.; Hallett, J. P. An Experimental Approach Probing the Conformational Transitions and Energy Landscape of Antibodies: A Glimmer of Hope for Reviving Lost Therapeutic Candidates Using Ionic Liquid. *Chem. Sci.* **2021**, *12*, 9528−9545.
(36) World Health Organization. *Health product and policy standards;* Health product and policy standards. World Health Organization https://www.who.int/teams/health-product-and-policy-standards/inn/inn-lists.
(37) *Craic Computing LLC. Tabs - Therapeutic Antibody Database*; Tabs - Therapeutic Antibody Database. https://tabs.craic.com/.
(38) Lefranc, M.-P.; Giudicelli, V.; Duroux, P.; Jabado-Michaloud, J.; Folch, G.; Aouinti, S.; Carillon, E.; Duvergey, H.; Houles, A.; Paysan-Lafosse, T.; Hadi-Saljoqi, S.; Sasorith, S.; Lefranc, G.; Kossida, S. IMGT®, the International ImMunoGeneTics Information System® 25 Years On. *Nucleic Acids Res.* **2015**, *43*, D413−D422.
(39) *Molecular Operating Environment (MOE), 2019.01*; 1010 Sherbooke St. West, Suite #910, Montreal, QC, Canada, H3A 2R7, 2021.
(40) Labute, P. The Generalized Born/Volume Integral Implicit Solvent Model: Estimation of the Free Energy of Hydration Using London Dispersion Instead of Atomic Surface Area. *J. Comput. Chem.* **2008**, *29*, 1693−1698.
(41) Labute, P. Protonate3D: Assignment of Ionization States and Hydrogen Coordinates to Macromolecular Structures. *Proteins Struct. Funct. Bioinf.* **2009**, *75*, 187−205.
(42) Stewart, D. E.; Sarkar, A.; Wampler, J. E. Occurrence and Role Ofcis Peptide Bonds in Protein Structures. *J. Mol. Biol.* **1990**, *214*, 253−260.
(43) Phillips, J. C.; Hardy, D. J.; Maia, J. D. C.; Stone, J. E.; Ribeiro, J. V.; Bernardi, R. C.; Buch, R.; Fiorin, G.; Hénin, J.; Jiang, W.; McGreevy, R.; Melo, M. C. R.; Radak, B. K.; Skeel, R. D.; Singharoy, A.; Wang, Y.; Roux, B.; Aksimentiev, A.; Luthey-Schulten, Z.; Kalé, L. V.; Schulten, K.; Chipot, C.; Tajkhorshid, E. Scalable Molecular Dynamics on CPU and GPU Architectures with NAMD. *J. Chem. Phys.* **2020**, *153*, No. 044130.
(44) Huang, J.; Rauscher, S.; Nawrocki, G.; Ran, T.; Feig, M.; de Groot, B. L.; Grubmüller, H.; MacKerell, A. D. CHARMM36m: An Improved Force Field for Folded and Intrinsically Disordered Proteins. *Nat. Methods* **2017**, *14*, 71−73.
(45) Jorgensen, W. L.; Chandrasekhar, J.; Madura, J. D.; Impey, R. W.; Klein, M. L. Comparison of Simple Potential Functions for Simulating Liquid Water. *J. Chem. Phys.* **1983**, *79*, 926−935.
(46) Darden, T.; York, D.; Pedersen, L. Particle Mesh Ewald: An N · log(N) Method for Ewald Sums in Large Systems. *J. Chem. Phys.* **1993**, *98*, 10089−10092.
(47) Ryckaert, J.-P.; Ciccotti, G.; Berendsen, H. J. C. Numerical Integration of the Cartesian Equations of Motion of a System with Constraints: Molecular Dynamics of n-Alkanes. *J. Comput. Phys.* **1977**, *23*, 327−341.
(48) Martyna, G. J.; Tobias, D. J.; Klein, M. L. Constant Pressure Molecular Dynamics Algorithms. *J. Chem. Phys.* **1994**, *101*, 4177−4189.
(49) Feller, S. E.; Zhang, Y.; Pastor, R. W.; Brooks, B. R. Constant Pressure Molecular Dynamics Simulation: The Langevin Piston Method. *J. Chem. Phys.* **1995**, *103*, 4613−4621.
(50) Humphrey, W.; Dalke, A.; Schulten, K. VMD: Visual Molecular Dynamics. *J. Mol. Graph.* **1996**, *14*, 33−38.
(51) Levine, B. G.; Stone, J. E.; Kohlmeyer, A. Fast Analysis of Molecular Dynamics Trajectories with Graphics Processing Units—Radial Distribution Function Histogramming. *J. Comput. Phys.* **2011**, *230*, 3556−3569.
(52) Berman, H. M.; Westbrook, J.; Feng, Z.; Gilliland, G.; Bhat, T. N.; Weissig, H.; Shindyalov, I. N.; Bourne, P. E. The Protein Data Bank. *Nucleic Acids Res.* **2000**, *28*, 235−242.
(53) Talavera, A.; Friemann, R.; Gómez-Puerta, S.; Martinez-Fleites, C.; Garrido, G.; Rabasa, A.; López-Requena, A.; Pupo, A.; Johansen, R. F.; Sánchez, O.; Krengel, U.; Moreno, E. Nimotuzumab, an Antitumor Antibody That Targets the Epidermal Growth Factor Receptor, Blocks Ligand Binding While Permitting the Active Receptor Conformation. *Cancer Res.* **2009**, *69*, 5851−5859.
(54) Sastyarina, Y.; Firdaus, A. R. R.; Nafisah, Z.; Hardianto, A.; Yusuf, M.; Ramli, M.; Mutalib, A.; Soedjanaatmadja, U. M. Modeling and Molecular Dynamic Simulation of F(Ab′) 2 Fragment of Nimotuzumab for Lung Cancer Diagnostics. *Bioinf. Biol. Insights* **2021**, *15*, 117793222110021.
(55) Humani, T. S.; Martoprawiro, M. A.; Mutalib, A. Temperature and Stretching Effects on Complementarity Determining Regions (CDRs) Conformation and Stability of Nimotuzumab F(Ab)-Fragment. *Atom. Indones.* **2015**, *41*, 17−25.
(56) Dunbar, J.; Fuchs, A.; Shi, J.; Deane, C. M. ABangle: Characterising the VH−VL Orientation in Antibodies. *Protein Eng., Des. Sel.* **2013**, *26*, 611−620.
(57) Virtanen, P.; Gommers, R.; Oliphant, T. E.; Haberland, M.; Reddy, T.; Cournapeau, D.; Burovski, E.; Peterson, P.; Weckesser, W.; Bright, J.; van der Walt, S. J.; Brett, M.; Wilson, J.; Millman, K. J.; Mayorov, N.; Nelson, A. R. J.; Jones, E.; Kern, R.; Larson, E.; Carey, C. J.; Polat, İ.; Feng, Y.; Moore, E. W.; VanderPlas, J.; Laxalde, D.; Perktold, J.; Cimrman, R.; Henriksen, I.; Quintero, E. A.; Harris, C. R.; Archibald, A. M.; Ribeiro, A. H.; Pedregosa, F.; van Mulbregt, P.; Contributors, S. 1 0; Vijaykumar, A.; Bardelli, A. P.; Rothberg, A.; Hilboll, A.; Kloeckner, A.; Scopatz, A.; Lee, A.; Rokem, A.; Woods, C. N.; Fulton, C.; Masson, C.; Häggström, C.; Fitzgerald, C.; Nicholson, D. A.; Hagen, D. R.; Pasechnik, D. V.; Olivetti, E.; Martin, E.; Wieser, E.; Silva, F.; Lenders, F.; Wilhelm, F.; Young, G.; Price, G. A.; Ingold, G.-L.; Allen, G. E.; Lee, G. R.; Audren, H.; Probst, I.; Dietrich, J. P.; Silterra, J.; Webber, J. T.; Slavič, J.; Nothman, J.; Buchner, J.; Kulick, J.; Schönberger, J. L.; Cardoso, J. V. d. M.; Reimer, J.; Harrington, J.; Rodríguez, J. L. C.; Nunez-Iglesias, J.; Kuczynski, J.; Tritz, K.; Thoma, M.; Newville, M.; Kümmerer, M.; Bolingbroke, M.; Tartre, M.; Pak, M.; Smith, N. J.; Nowaczyk, N.; Shebanov, N.; Pavlyk, O.; Brodtkorb, P. A.; Lee, P.; McGibbon, R. T.; Feldbauer, R.; Lewis, S.; Tygier, S.; Sievert, S.; Vigna, S.; Peterson, S.; More, S.; Pudlik, T.; Oshima, T.; Pingel, T. J.; Robitaille, T. P.; Spura, T.; Jones, T. R.; Cera, T.; Leslie, T.; Zito, T.; Krauss, T.; Upadhyay, U.; Halchenko, Y. O.; Vázquez-Baeza, Y. SciPy 1.0: Fundamental Algorithms for Scientific Computing in Python. *Nat. Methods* **2020**, *17*, 261−272.
(58) Krehbiel, T. C. Correlation Coefficient Rule of Thumb. *Decis. Sci. J. Innov* **2004**, *2*, 97−100.
(59) Arosio, P.; Barolo, G.; Müller-Späth, T.; Wu, H.; Morbidelli, M. Aggregation Stability of a Monoclonal Antibody During Downstream Processing. *Pharm. Res.* **2011**, *28*, 1884−1894.
(60) Nishigami, H.; Kamiya, N.; Nakamura, H. Revisiting Antibody Modeling Assessment for CDR-H3 Loop. *Protein Eng., Des. Sel.* **2016**, *29*, 477−484.

https://doi.org/10.1021/acs.molpharmaceut.2c00838
Mol. Pharmaceutics 2023, 20, 1096−1111

(61) Fernández-Quintero, M. L.; Loeffler, J. R.; Kraml, J.; Kahler, U.; Kamenik, A. S.; Liedl, K. R. Characterizing the Diversity of the CDR-H3 Loop Conformational Ensembles in Relationship to Antibody Binding Properties. *Front. Immunol.* **2019**, *9*, 3065.
(62) Waibl, F.; Fernández-Quintero, M. L.; Kamenik, A. S.; Kraml, J.; Hofer, F.; Kettenberger, H.; Georges, G.; Liedl, K. R. Conformational Ensembles of Antibodies Determine Their Hydrophobicity. *Biophys. J.* **2021**, *120*, 143−157.
(63) Salgado, J. C.; Rapaport, I.; Asenjo, J. A. Predicting the Behaviour of Proteins in Hydrophobic Interaction Chromatography 1: Using the Hydrophobic Imbalance (HI) to Describe Their Surface Amino Acid Distribution. *J. Chromatogr., A* **2006**, *1107*, 110−119.
(64) Knapp, B.; Dunbar, J.; Alcala, M.; Deane, C. M. Variable Regions of Antibodies and T-Cell Receptors May Not Be Sufficient in Molecular Simulations Investigating Binding. *J. Chem. Theory Comput.* **2017**, *13*, 3097−3105.
(65) Tomar, D. S.; Licari, G.; Bauer, J.; Singh, S. K.; Li, L.; Kumar, S. Stress-Dependent Flexibility of a Full-Length Human Monoclonal Antibody: Insights from Molecular Dynamics to Support Biopharmaceutical Development. *J. Pharm. Sci.* **2022**, *111*, 628−637.
(66) Fernández-Quintero, M. L.; Hoerschinger, V. J.; Lamp, L. M.; Bujotzek, A.; Georges, G.; Liedl, K. R. VH-VL Interdomain Dynamics Observed by Computer Simulations and NMR. *Proteins Struct. Funct. Bioinf.* **2020**, *88*, 830−839.
(67) Mei, Z.; Treado, J. D.; Grigas, A. T.; Levine, Z. A.; Regan, L.; O'Hern, C. S. Analyses of Protein Cores Reveal Fundamental Differences between Solution and Crystal Structures. *Proteins Struct. Funct. Bioinf.* **2020**, *88*, 1154−1161.
(68) Murakawa, T.; Baba, S.; Kawano, Y.; Hayashi, H.; Yano, T.; Kumasaka, T.; Yamamoto, M.; Tanizawa, K.; Okajima, T. In Crystallo Thermodynamic Analysis of Conformational Change of the Topaquinone Cofactor in Bacterial Copper Amine Oxidase. *Proc. Natl. Acad. Sci.* **2019**, *116*, 201811837.
(69) Chi, E. Y.; Krishnan, S.; Randolph, T. W.; Carpenter, J. F. Physical Stability of Proteins in Aqueous Solution: Mechanism and Driving Forces in Nonnative Protein Aggregation. *Pharm. Res.* **2003**, *20*, 1325−1336.
(70) Salis, A.; Monduzzi, M. Not Only PH. Specific Buffer Effects in Biological Systems. *Curr. Opin. Colloid Interface Sci.* **2016**, *23*, 1−9.
(71) Carpenter, J. F.; Kendrick, B. S.; Chang, B. S.; Manning, M. C.; Randolph, T. W. [16] Inhibition of Stress-Induced Aggregation of Protein Therapeutics. *Methods Enzymol.* **1999**, *309*, 236−255.
(72) Manning, M. C.; Liu, J.; Li, T.; Holcomb, R. E. Rational Design of Liquid Formulations of Proteins. *Adv. Protein Chem. Struct. Biol.* **2018**, *112*, 1−59.
(73) Wälchli, R.; Ressurreição, M.; Vogg, S.; Feidl, F.; Angelo, J.; Xu, X.; Ghose, S.; Li, Z. J.; Saoût, X. L.; Souquet, J.; Broly, H.; Morbidelli, M. Understanding MAb Aggregation during Low PH Viral Inactivation and Subsequent Neutralization. *Biotechnol. Bioeng.* **2020**, *117*, 687−700.
(74) Lopez, E.; Scott, N. E.; Wines, B. D.; Hogarth, P. M.; Wheatley, A. K.; Kent, S. J.; Chung, A. W. Low PH Exposure During Immunoglobulin G Purification Methods Results in Aggregates That Avidly Bind Fcγ Receptors: Implications for Measuring Fc Dependent Antibody Functions. *Front. Immunol.* **2019**, *10*, 2415.
(75) Djoumerska-Alexieva, I. K.; Dimitrov, J. D.; Voynova, E. N.; Lacroix-Desmazes, S.; Kaveri, S. V.; Vassilev, T. L. Exposure of IgG to an Acidic Environment Results in Molecular Modifications and in Enhanced Protective Activity in Sepsis. *FEBS J.* **2010**, *277*, 3039−3050.
(76) Cloutier, T.; Sudrik, C.; Mody, N.; Sathish, H. A.; Trout, B. L. Molecular Computations of Preferential Interaction Coefficients of IgG1 Monoclonal Antibodies with Sorbitol, Sucrose, and Trehalose and the Impact of These Excipients on Aggregation and Viscosity. *Mol. Pharmaceutics* **2019**, *16*, 3657−3664.
(77) Jo, S.; Xu, A.; Curtis, J. E.; Somani, S.; MacKerell, A. D. Computational Characterization of Antibody−Excipient Interactions for Rational Excipient Selection Using the Site Identification by Ligand Competitive Saturation-Biologics Approach. *Mol. Pharmaceutics* **2020**, *17*, 4323−4333.
(78) Smiatek, J. Theoretical and Computational Insight into Solvent and Specific Ion Effects for Polyelectrolytes: The Importance of Local Molecular Interactions. *Molecules* **2020**, *25*, 1661.
(79) Zhang, Y.; Cremer, P. S. Interactions between Macromolecules and Ions: The Hofmeister Series. *Curr. Opin. Chem. Biol.* **2006**, *10*, 658−663.
(80) Collins, K. D.; Neilson, G. W.; Enderby, J. E. Ions in Water: Characterizing the Forces That Control Chemical Processes and Biological Structure. *Biophys. Chem.* **2007**, *128*, 95−104.
(81) Inaba, S.; Kamiya, N.; Bekker, G.-J.; Kawai, F.; Oda, M. Folding Thermodynamics of PET-Hydrolyzing Enzyme Cut190 Depending on Ca2+ Concentration. *J. Therm. Anal. Calorim.* **2019**, *135*, 2655−2663.
(82) Liu, J.; Wang, L.; Zhan, S. Y.; Xia, Y. Daclizumab for Relapsing Remitting Multiple Sclerosis. *Cochrane Database Syst Rev* **2013**, *12*, CD008127.
(83) Lycke, J. Monoclonal Antibody Therapies for the Treatment of Relapsing-Remitting Multiple Sclerosis: Differentiating Mechanisms and Clinical Outcomes. *Ther. Adv. Neurol. Disord.* **2015**, *8*, 274−293.
(84) Casaz, P.; Boucher, E.; Wollacott, R.; Pierce, B. G.; Rivera, R.; Sedic, M.; Ozturk, S.; Thomas, W. D., Jr.; Wang, Y. Resolving Self-Association of a Therapeutic Antibody by Formulation Optimization and Molecular Approaches. *mAbs* **2014**, *6*, 1533−1539.
(85) Hebditch, M.; Warwicker, J. Charge and Hydrophobicity Are Key Features in Sequence-Trained Machine Learning Models for Predicting the Biophysical Properties of Clinical-Stage Antibodies. *Peerj* **2019**, *7*, No. e8199.
(86) Kuhn, A. B.; Kube, S.; Karow-Zwick, A. R.; Seeliger, D.; Garidel, P.; Blech, M.; Schäfer, L. V. Improved Solution-State Properties of Monoclonal Antibodies by Targeted Mutations. *J. Phys. Chem. B* **2017**, *121*, 10818−10827.
(87) Shahfar, H.; Du, Q.; Parupudi, A.; Shan, L.; Esfandiary, R.; Roberts, C. J. Electrostatically Driven Protein−Protein Interactions: Quantitative Prediction of Second Osmotic Virial Coefficients to Aid Antibody Design. *J. Phys. Chem. Lett.* **2022**, *13*, 1366−1372.
(88) Yadav, S.; Laue, T. M.; Kalonia, D. S.; Singh, S. N.; Shire, S. J. The Influence of Charge Distribution on Self-Association and Viscosity Behavior of Monoclonal Antibody Solutions. *Mol. Pharmaceutics* **2012**, *9*, 791−802.
(89) Kuroda, D.; Tsumoto, K. Engineering Stability, Viscosity, and Immunogenicity of Antibodies by Computational Design. *J. Pharm. Sci.* **2020**, *109*, 1631−1651.
(90) Datta-Mannan, A.; Thangaraju, A.; Leung, D.; Tang, Y.; Witcher, D. R.; Lu, J.; Wroblewski, V. J. Balancing Charge in the Complementarity-Determining Regions of Humanized MAbs without Affecting PI Reduces Non-Specific Binding and Improves the Pharmacokinetics. *mAbs* **2015**, *7*, 483−493.
(91) Jetha, A.; Thorsteinson, N.; Jmeian, Y.; Jeganathan, A.; Giblin, P.; Fransson, J. Homology Modeling and Structure-Based Design Improve Hydrophobic Interaction Chromatography Behavior of Integrin Binding Antibodies. *mAbs* **2018**, *10*, 890−900.
(92) Gupta, P.; Makowski, E. K.; Kumar, S.; Zhang, Y.; Scheer, J. M.; Tessier, P. M. Antibodies with Weakly Basic Isoelectric Points Minimize Trade-Offs between Formulation and Physiological Colloidal Properties. *Mol. Pharmaceutics* **2022**, 775.
(93) Choi, Y.; Ndong, C.; Griswold, K. E.; Bailey-Kellogg, C. Computationally Driven Antibody Engineering Enables Simultaneous Humanization and Thermostabilization. *Protein Eng., Des. Sel.* **2016**, *29*, 419−426.
(94) Bauer, J.; Mathias, S.; Kube, S.; Otte, K.; Garidel, P.; Gamer, M.; Blech, M.; Fischer, S.; Karow-Zwick, A. R. Rational Optimization of a Monoclonal Antibody Improves the Aggregation Propensity and Enhances the CMC Properties along the Entire Pharmaceutical Process Chain. *mAbs* **2020**, *12*, 1787121.
(95) Melien, R.; Garidel, P.; Hinderberger, D.; Blech, M. Thermodynamic Unfolding and Aggregation Fingerprints of Monoclonal Antibodies Using Thermal Profiling. *Pharm. Res.* **2020**, *37*, 78.
(96) Seeliger, D.; Schulz, P.; Litzenburger, T.; Spitz, J.; Hoerer, S.; Blech, M.; Enenkel, B.; Studts, J. M.; Garidel, P.; Karow, A. R. Boosting

Antibody Developability through Rational Sequence Optimization. *mAbs* **2015**, *7*, 505−515.
(97) Fuh, G.; Wu, P.; Liang, W.-C.; Ultsch, M.; Lee, C. V.; Moffat, B.; Wiesmann, C. Structure-Function Studies of Two Synthetic Anti-Vascular Endothelial Growth Factor Fabs and Comparison with the Avastin™ Fab*. *J Biol Chem* **2006**, *281*, 6625−6631.
(98) Niu, B.; Martinelli, M., II; Jiao, Y.; Wang, C.; Cao, M.; Wang, J.; Meinke, E. Nonspecific Cleavages Arising from Reconstitution of Trypsin under Mildly Acidic Conditions. *PLoS One* **2020**, *15*, No. e0236740.
(99) Gokarn, Y.; Agarwal, S.; Arthur, K.; Bepperling, A.; Day, E. S.; Filoti, D.; Greene, D. G.; Hayes, D.; Kroe-Barrett, R.; Laue, T.; Lin, J.; McGarry, B.; Razinkov, V.; Singh, S.; Taing, R.; Venkataramani, S.; Weiss, W.; Yang, D.; Zarraga, I. E. *State-of-the-Art and Emerging Technologies for Therapeutic Monoclonal Antibody Characterization Volume 2. Biopharmaceutical Characterization: The NISTmAb Case Study*; American Chemical Society. 2015, 285−327.
(100) Saro, D.; Baker, A.; Hepler, R.; Spencer, S.; Bruce, R.; LaBrenz, S.; Chiu, M.; Davis, D.; Lang, S. E. *State-of-the-Art and Emerging Technologies for Therapeutic Monoclonal Antibody Characterization Volume 2. Biopharmaceutical Characterization: The NISTmAb Case Study*; American Chemical Society 2015, 329−355.
(101) Jin, W.; Xing, Z.; Song, Y.; Huang, C.; Xu, X.; Ghose, S.; Li, Z. J. Protein Aggregation and Mitigation Strategy in Low PH Viral Inactivation for Monoclonal Antibody Purification. *mAbs* **2019**, *11*, 1479−1491.
(102) Marunych, R. Y.; Hrabovskyi, O. O.; Bereznytskyj, G. K.; Pyrogova, L. V.; Gogolinskaya, G. K.; Makogonenko, Y. M. Chlorine-Binding Structures: Role and Organization in Different Proteins. *Ukr. Biochem. J.* **2021**, *93*, 5−17.
(103) Timasheff, S. N. Control of Protein Stability and Reactions by Weakly Interacting Cosolvents: The Simplicity of the Complicated. *Adv. Protein Chem.* **1998**, *51*, 355−432.
(104) Maclean, D. S.; Qian, Q.; Middaugh, C. R. Stabilization of Proteins by Low Molecular Weight Multi-ions. *J. Pharm. Sci.* **2002**, *91*, 2220−2229.

https://doi.org/10.1021/acs.molpharmaceut.2c00838
Mol. Pharmaceutics 2023, 20, 1096−1111